Advanced Powder Technology 34 (2023) 104010

Contents lists available at ScienceDirect

Advanced Powder Technology

journal homepage: www.elsevier.com/locate/apt

Experimental assessments of pyrolytic and fluid-dynamic interactions between pretreated residual biomasses and fluidized beds made up of oxygen carriers for chemical looping gasification

Andrea Di Giuliano *, Barbara Malsegna, Stefania Lucantonio, Katia Gallucci

Department of Industrial and Information Engineering and Economics (DIIIE), University of L'Aquila, Piazzale E.Pontieri 1-loc., Monteluco di Roio, 67100 L'Aquila, Italy

ARTICLE INFO

Article history:
Received 30 August 2022
Received in revised form 9 February 2023
Accepted 13 March 2023

Keywords:
Torrefaction
Washing
Chemical looping gasification
Devolatilization
Fluidization
Mineral-addition

ABSTRACT

Oxygen carriers (OCs) and wheat straw pellets (raw or pretreated by combinations of torrefaction, $CaCO_3$-addition, water-washing) were experimentally investigated for Chemical Looping Gasification (CLG) in the Horizon2020 project CLARA (Chemical Looping gAsification foR sustAinable production of biofuels, grant agreement n.817841). Laboratory-scale experiments included: (i) pellet devolatilizations (700 °C-900 °C) in bubbling fluidized beds made of OCs or sand; (ii) study of pressure fluctuations within OC fluidized beds (700–1000 °C) containing 10 vol% of ashes from investigated pellets, to assess OC/ash interactions and fluidization quality. Those two campaigns – performed at relevant process conditions for CLG – allowed straightforwardly screening and selecting the most eligible biomasses and OCs for future CLG demonstrations in fluidized beds at higher scales. Gas yield, H_2/CO molar ratio, and carbon conversion increased as the devolatilization temperature increased from 700 °C to 900°C. Untreated and pretreated wheat straw pellets showed different pyrolytic behaviors. Analyses of pressure fluctuations and characterizations of spent beds (scanning electron microscopy, particle size distribution) suggested that biomass pretreatments limit agglomeration phenomena, depending on OCs nature (e.g., mechanical strength, composition). Ilmenite was the most mechanically and chemically stable OC. Among investigated materials, pretreated wheat straw pellets and ilmenite emerged as the most promising for future CLG demonstrations.

1. Introduction

Negative Emissions Technologies (NET) include those technologies or actions that allow for decreasing the concentration of greenhouse gases in the atmosphere [1,2]. NET have attracted increasing interest; in the 2018 special report from United Nations Intergovernmental Panel on Climate Change (IPCC) on global warming containment at + 1.5 °C, the outlined scenarios rely on the net removal of CO_2 from the atmosphere [3].

BioEnergy with Carbon Capture and Storage (BECCS) – i.e., the use of biomass for energy purposes coupled with Carbon Capture and Storage (CCS) – emerged as a candidate NET [2,4]. Biomass is a potentially carbon–neutral fuel, since the CO_2 produced by its combustion has previously been removed from the atmosphere by photosynthesis [5]; therefore, the combination of biomass conversion with CCS might result in a NET [6].

Chemical looping technologies fed with biomasses are promising BECCS applications, since it is estimated that they involve the lowest energy and cost penalties associated with CO_2 capture [7–9]. The use of so-called Oxygen Carriers (OCs) is the technological breakthrough of chemical looping, enabling the process intensification of related thermochemical conversions: OCs are solid materials typically containing metal oxides with redox properties, that act as intermediaries in chemical reactions between fuels and oxidants, by releasing or acquiring lattice oxygen (redox behavior) [10,11].

Dual interconnected fluidized bed reactors that host a granular OC as the internally circulated solid [12–18] have been proposed in many chemical looping applications, even up to the MW_{th} scale: (i) in one vessel (fuel reactor), the biomass is converted while the fluidized OC releases its lattice oxygen; (ii) in the other vessel (air reactor), the reduced OC is re-oxidized by air-combustion; (iii) the reduced OC is returned into the fuel reactor, also transferring part of the heat of combustion as sensible heat. Further details can be found in the literature about dual interconnected fluidized beds applied to gasification [19] or chemical looping [20,21].

* Corresponding author.
E-mail address: andrea.digiuliano@univaq.it (A. Di Giuliano).

https://doi.org/10.1016/j.apt.2023.104010

Chemical Looping Gasification (CLG) brings together the advantages of CCS pre-combustion [22] and oxy-fuel-combustion [23,24] technologies, allowing the production of undiluted syngas (mainly H_2/CO mixture) without the use of expensive air separation units [8,25,26]. That undiluted syngas can be converted into liquid fuels by catalytic conversions [27,28], leading to biofuel synthesis in the case of CLG based on biomasses [27,29].

The origin of fed biomass is not of secondary importance in the overall impact of the process, as it is related to forest reduction, degradation of productive lands, intensification of energy-crops production, and competition with food chains [30]. Residual biomasses (also known as biogenic residues) can work as renewable feedstocks to produce sustainable, valuable chemicals and second-generation biofuels (not competing with food chains) [31,32]. Wheat straw is attractive among lignocellulosic biogenic residues thanks to its extensive availability [33]. Unfortunately, wheat straw brings in potential issues related to fluidization quality, because of sintering and ash agglomeration or melting [34–36], due to the high content of low-melting mineral matter [37–39], such as alkali and alkali earths [6,35,40–42]. In order to improve biomass properties (e.g., energy density, the content of polluting elements) and avoid process issues (e.g., downstream contaminations, ash/OCs agglomeration), biomass pretreatments were proposed in the literature, such as torrefaction [41,43–48], washing with water [41,43,44,49–51] and addition of minerals [36,52]. It is worth noting that pretreatments can also affect the performance of biomasses in thermochemical conversions [6,41,43,44].

The ongoing Horizon 2020 European research project CLARA (Chemical Looping gAsification foR sustAinable production of biofuels, grant agreement n. 817841 [53]) was born in this framework, and data presented in this work belong to the related research. Since November 2018, CLARA has investigated the use of wheat straw pellets (pretreated by torrefaction, water-washing, mineral addition) as solid fuels for CLG in fluidized beds made of natural or waste-derived OCs; in terms of novelty, CLARA is the only European project dealing with CLG [54] and it has the final aim of performing the first demonstration of a full biomass-to-fuel-chain based on the CLG of wheat straw by a dual interconnected fluidized bed reactor at 1 MW_{th} scale, followed by a Fischer-Tropsch step [53]. This is an ambitious goal, considering that CLG has never been performed beyond the laboratory scales up to 25 kW_{th} [55,56], to the best of the authors' knowledge of literature. A crucial step before the final demonstration is the preliminary choice of the most eligible fuels and OCs for CLG. To fill this gap, this work applies manageable methodologies at a laboratory-scale on novel pretreated wheat straw biomasses and OCs of interest in terms of sustainability, as they are natural mineral ores or waste-derived materials. Generally, the choice of feedstock and materials to be tested at demonstrative scales needs a previous understanding of their behaviors under industrially relevant conditions, to avoid unsuccessful demonstrations, as well as loss of money and trust in the developed technology.

Experiments and results discussed in this manuscript cover this need, having the scope of understanding the behaviors of pellets derived from wheat straw and natural or waste-derived OCs, at process conditions relevant to CLG in a fluidized bed. Seven kinds of wheat straw pellets (raw; pretreated by torrefaction and $CaCO_3$ addition; pretreated by torrefaction, $CaCO_3$ addition, and water-washing) and three OCs (natural mineral ores or waste-derived materials) were considered. The $CaCO_3$-added wheat straw pellets were never investigated by this research group. The assessments of their pyrolytic and fluid-dynamic behaviors were performed by two dedicated laboratory-scale experimental campaigns at relevant conditions for CLG: (i) devolatilization tests of pellets dropped in OCs fluidized beds; (ii) pressure fluctuation tests in fluidized beds composed of ash from biomass pellets and one OC, to assess fluidization quality.

As a step of gasification [57], devolatilization contributes to determine the quantity and quality of developed syngas [58]. At the usual high temperatures of gasification, and CLG as well, the vapors and tars produced in the primary devolatilization step are converted by secondary reactions into additional gaseous and solid products [58,59]. When fed to a gasifying fluidized bed, the particles of a solid fuel experience fast chemical and morphological changes due to [58,60,61]: (i) the abrupt heating from the feeding temperature to the bed one; (ii) the simultaneous occurrence of drying, devolatilization, and secondary reactions; (iii) the complex fluid-dynamic interactions involving fluidizing/gasification agents (e.g., steam, air), reaction products, bed particles, fuel particles, and solid residuals. As a consequence of those peculiar conditions, technical choices and predictions about the thermochemical conversion of biomasses within industrial fluidized beds should follow experiments in the same kind of reactors; extrapolations from results obtained by different reactor configurations (e.g., laboratory thermogravimetric analyses, packed beds) could turn out to be unfit for this purpose [58,62–64]. In light of those observations, this work presents experiments of devolatilizations in fluidized beds with pellets drop, that enabled the quantification of pyrolytic behavior of novel wheat straw pellets interacting with OCs.

Concerning fluid-dynamic behavior, the intrinsically heterogeneous state of bubbling fluidized beds and their instantaneous pressure fluctuations are strongly related [34], so the analyses of pressure signals (e.g., time series analyses, frequency-domain analyses, chaotic invariants and dynamic moments) emerged in the literature as diagnostic tools to assess the fluidization quality in cold-models [65–69], bench-scale [70,71], and pilot-scale reactors [40]; those analyses were also evaluated for scalability to industrial reactors [35,72,73]. This research group's experience focuses on studying dominant frequencies in the Power Spectral Density Function (PSDF) and standard deviations of pressure fluctuation signals [65,66,74]. This work applies the study of pressure fluctuation signals to laboratory-scale fluidized beds made of OCs and ashes from wheat straw pellets, operated at relevant temperatures for CLG. The aim is to monitor the stability of the bubbling fluidization quality of OCs in the presence of potential causes of defluidization (e.g., agglomeration-triggering elements from biomass ashes or cohesive behaviors of particles).

In the following, this work quantifies pyrolytic behaviors and evaluates fluid-dynamic aspects of novel lignocellulosic biomasses interacting with potentially sustainable OCs, at conditions relevant for CLG, in order to evaluate the effectiveness of the investigated biomass pretreatments, and choose the most promising materials to demonstrate in the next future the CLG of pretreated wheat straw at the MW_{th} scale for the first time, in the framework of the project CLARA.

2. Materials and methods

2.1. Biomasses

The two experimental campaigns investigated seven formulations of biomass pellets: raw wheat straw pellets; wheat straw pellets torrefied at three temperatures, with added $CaCO_3$; wheat straw pellets torrefied and at three temperatures and washed (water-leaching), with added $CaCO_3$. $CaCO_3$ additive was provided by Forschungszentrum Jülich GmbH (Germany) to CENER (Centro Nacional de Energías Renovables, Spain), that in turn produced the pretreated pellets (both partners of the CLARA project). $CaCO_3$ corresponded to 2 wt% of the pretreated biomass [75], whereas fur-

ther details about torrefaction and water-washing can be found elsewhere [6].

Table 1 shows the names and associated pretreatments of the seven biomasses studied in this work. These biomasses were characterized by proximate and ultimate analyses, which allowed determining the moisture and ash contents, and their elemental composition, all used in calculations described in Section 2.3; some of these measurements are available in [75–77].

2.2. Oxygen carriers (OCs)

Three OCs were investigated: (i) ilmenite (ILM), a natural iron and titanium mineral [6,41,78,79]; (ii) calcined "Sibelco" (SIB), a natural iron and manganese ore [6,41]; (iii) Linz-Donawitz slag (LD), mainly containing iron, manganese, and calcium [6,13,41,80,81]. The chemical composition of those OCs was reported elsewhere [6,75]. As previously determined by this research group, all the OC samples used in this work belong to the generalized Geldart B group [34] at all tested conditions, i.e., their minimum fluidization velocity coincides with their minimum bubbling velocity [6,34]. The minimum fluidization velocities (u_{mf}) of OCs at all conditions tested in this work can be found elsewhere [6].

2.3. Devolatilization tests

Devolatilization tests were carried out in a quartz fluidized bed reactor (Fig. 1(a)), at three temperatures representative of gasification (700 °C, 800 °C, 900 °C) with N_2 as the fluidizing gas, at 1.5 times the minimum fluidization velocity (u_{mf}) of the tested bed material, to ensure similar fluid-dynamic conditions for all devolatilizations. The devolatilized syngas was cooled, dried, and analyzed to determine the volumetric concentration of H_2, CO, CO_2, CH_4, and hydrocarbons (expressed as equivalent C_3H_8, $C_3H_{8,eq}$) (Fig. 1(a)). Pellets of all biomasses in Table 1 were devolatilized in bubbling fluidized beds made of one of the three OCs (see Section 2.2) or inert sand. The sand samples belong to the generalized Geldart B group [61]. The u_{mf} values for ILM, SIB, LD, and sand were reported elsewhere [61].

Each pellet was devolatilized individually, and the following was fed into the reactor only when the devolatilization of the previous ended; so, the process was carried out in an unsteady-state condition.

According to mass conservation principles, assuming the N_2 flow as the internal standard and thanks to measurements of volumetric concentrations, instantaneous outlet molar flow rates of syngas components as functions of time (t) were determined ($F_{i,out}$ with i = H_2, CO, CO_2, CH_4, $C_3H_{8,eq}$). Then, integral-average parameters were calculated from experimental measurements: (i) gas yield η^{av} (Equation 1); (ii) H_2/CO molar ratio λ^{av} (Equation 2); (iii) carbon conversion χ_C^{av} (Equation 3); molar fractions on dry, N_2-free basis Y_i^{av}, with i = H_2, CO, CO_2, CH_4, $C_3H_{8,eq}$ (Equation 4).

$$\eta^{av} = \frac{\sum_i \int F_{i,out}\, dt}{m_p}$$

$$with\ i = H_2,\ CO,\ CO_2,\ CH_4\ and\ C_3H_{8,eq}$$

(Equation 1).

$$\lambda^{av} = \frac{\int F_{H_2,out}\, dt}{\int F_{CO,out}\, dt}$$

(Equation 2).

$$\chi_C{}^{av} = \frac{12\left(g\,mol^{-1}\right)\cdot \sum_j [n_j \cdot \int F_{j,out}\, dt]}{m_p \cdot \left(1 - \frac{\%moisture_{ar}}{100}\right)\cdot \left(1 - \frac{\%ash_{db}}{100}\right)\cdot \left(\frac{\%C_{daf}}{100}\right)} \cdot 100$$

$$with\ j = CO,\ CO_2,\ CH_4\ and\ C_3H_{8,eq}$$

(Equation 3).

$$Y_i^{av} = \frac{\int F_{i,out}\, dt}{\sum_j \int F_{j,out}\, dt} 100$$

$$with\ j = H_2,\ CO,\ CO_2,\ CH_4\ and\ C_3H_{8,eq}$$

(Equation 4).

Those parameters allowed assessing and uniformly comparing the devolatilization performances of pellets under different conditions. Three replications were performed for each set of "biomass/bed material/devolatilization temperature" in a complete and balanced experimental plan.

Other details about the experimental apparatus, procedures, and data calculations are described elsewhere [43].

2.4. Pressure fluctuation tests and characterizations after-tests

A fluidized suspension can be assumed to be in a quasi-stationary state, having physical properties with mean values that are time-independent over a finite period (ergodic signal) [82], so pressure fluctuation signals of finite duration can be studied [6].

The signals of dynamic pressure fluctuations were acquired in beds made of one OC (90 ml bulk volume) coupled with 10 vol% of ash (10 ml bulk volume) from one biomass (Table 1) at temperatures of interest for CLG, including OC regeneration (700 °C, 750 °C, 800 °C, 850 °C, 900 °C, 950 °C, 1000 °C), using N_2 as the fluidizing agent at superficial velocity (u) equaling 2 and 3 times the u_{mf} of the selected OC. For each set of "u/bed temperature/OC/biomass ash" two replications of the signal acquisition were performed.

Those mixings are named "*OC/ash(biomass)*". E.g., LM/ash(WSP-T1Wadd) is the mixing of 90 ml of ILM with 10 vol% of ashes from WSP-T1Wadd (Table 1).

Bed inventories were fluidized in a heated quartz cylindrical vertical reactor, with a pressure probe submerged in the fluidized bed (Fig. 1b). The probe was connected to a piezoelectric pressure transducer, which transmitted its signal to an integrated charge-amplifier/digital-converter KISTLER 5165A (Fig. 1b). Digitalized pressure fluctuation signals were studied by a purposely developed MATLAB® script, that corrected the drift of signals, then determined the standard deviation of corrected pressure fluctuation signals ($\sigma_{\Delta P}$) and their Power Spectral Density Functions (PSFD).

Each acquisition lasted for 163.84 s with a sampling frequency of 100 Hz. Those settings resulted from precautions needed to ensure the reliability of signals and their applicability to calculate

Table 1
Biomasses investigated with the specification of the related pretreatments.

Name of Biomass	Biomass features
WSP	Wheat Straw Pellet (raw)
WSP-T1add	Wheat Straw Pellet-Torrefied at T1 = 250 °C, with 2 wt% $CaCO_3$
WSP-T2add	Wheat Straw Pellet-Torrefied at T2 = 260 °C, with 2 wt% $CaCO_3$
WSP-T3add	Wheat Straw Pellet-Torrefied at T3 = 270 °C, with 2 wt% $CaCO_3$
WSP-T1Wadd	Wheat Straw Pellet-Torrefied at T1 and Washed, with 2 wt % $CaCO_3$
WSP-T2Wadd	Wheat Straw Pellet-Torrefied at T2 and Washed, with 2 wt % $CaCO_3$
WSP-T3Wadd	Wheat Straw Pellet-Torrefied at T3 and Washed, with 2 wt % $CaCO_3$

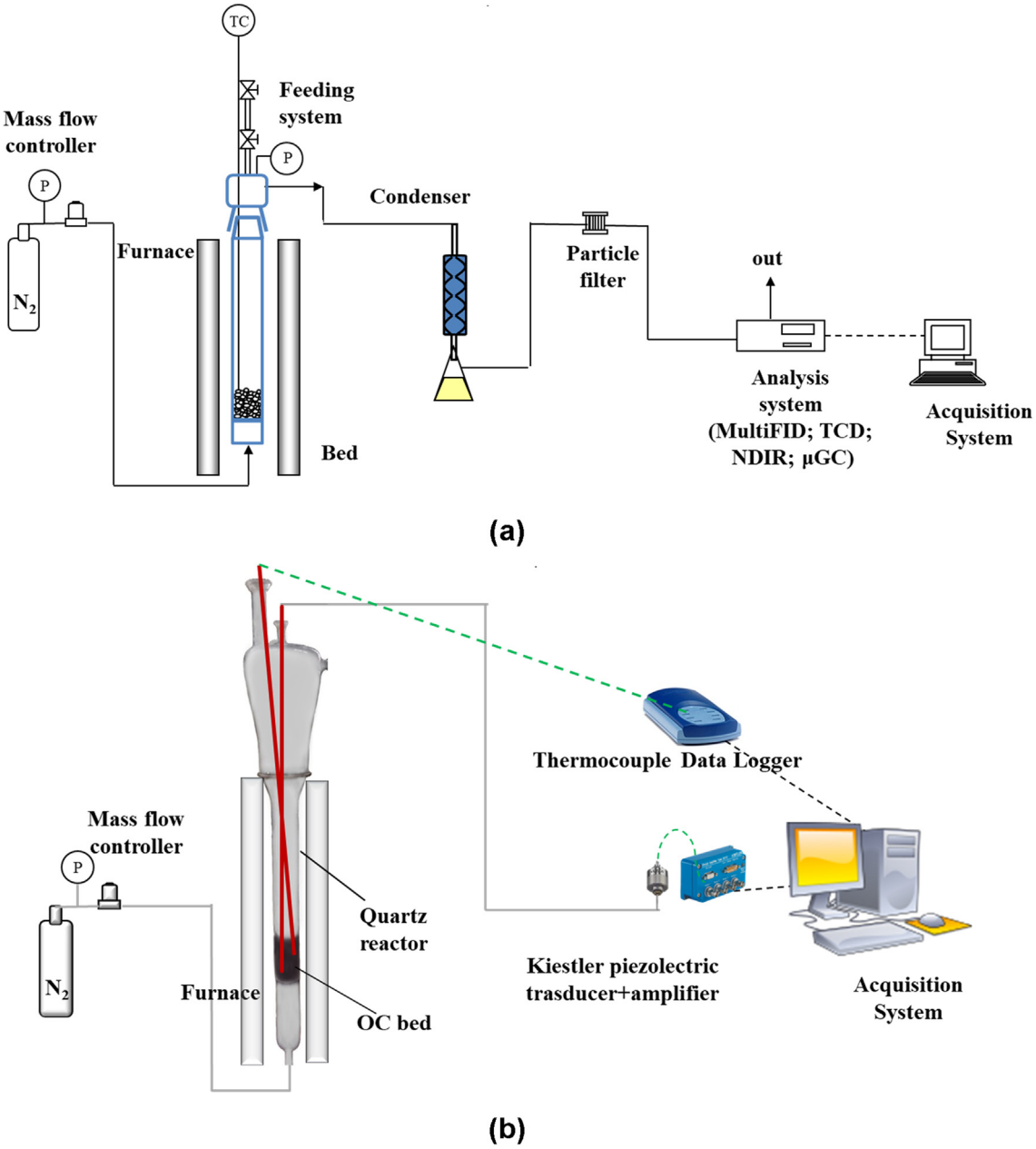

Fig. 1. Schematic view of the laboratory-scale experimental rigs: for pyrolysis tests (adapted from [61]) (a); for pressure fluctuation tests (reproduced from [6]).

PSDF: (i) the sampling frequency was chosen to fulfill the requirements of the Nyquist theorem; (ii) in order to be statistically significant, pressure fluctuation signals must count at least 10,000 points [83]; (iii) the number of points must be a power of 2 in order to apply the fast Fourier transform needed to calculate the PSDF (2^{14} = 16,384 is the lowest power of 2 higher than 10,000). The beds underwent fluidization with ash at each temperature for durations between 30 and 60 min, to ensure a complete exposure to relevant process conditions.

The joint evaluation of $\sigma_{\Delta P}$ and locally dominant frequencies in the PSDFs indicated whether bubbling fluidization – the only one possible for Geldart B systems at u close to u_{mf} [34] – occurred during the tests. The amplitude of pressure fluctuations, quantified by $\sigma_{\Delta P}$, mainly depends on the bed oscillations in turn induced by the erupting bubbles [84]; the locally dominant frequency in the PSDF (order of 10^0 Hz for bubbling beds) is related to the number of erupting bubbles [85,86]. Therefore, the decrease of both locally dominant frequencies of the PSDF (associated with the number of bubbles) and $\sigma_{\Delta P}$ of their parent signals of pressure fluctuation (related to the dimension of bubbles) can evidence the disappearance of bubbles [6].

In addition to the study of pressure fluctuation signals, selected bed samples were characterized before and after the tests of pressure fluctuation acquisitions, to assess possible variations of particle properties at the process conditions relevant to the CLG. Characterization methods included: Scanning Electron Microscopy (SEM) coupled with Energy Dispersive X-ray Spectrometry (EDS) for elemental analysis by a properly equipped GeminiSEM 500 microscope; measurement of Particle Size Distributions (PSDs) and average particle diameters (d_p) by laser diffraction Malvern Mastersizer 2000 analyzer.

Other details about experimental procedures, mathematical elaboration of signals, and related theoretical references are described elsewhere [6].

3. Results and discussion

3.1. Devolatilization tests

Data that quantifies the isolated step of devolatilization, at usual gasification temperatures and relevant reaction configuration (i.e., bubbling bed) is valuable for those researchers interested in biomass CLG or just gasification (thanks to experiments with the sand bed) from both experimental and modeling points of view.

Tables in Appendix A show arithmetic means of η^{av}, λ^{av}, and χ_C^{av} and related standard deviations out of the three replications per each set of conditions "biomass/bed material/devolatilization temperature" exerted in the devolatilization experimental campaign (a total of 252 devolatilizations). The same values were discussed in this Section and graphically summarized in Fig. 2, Fig. 3, and Fig. 4. Fig. 2 gives an overall view of trends concerning arithmetic means of η^{av}, λ^{av}, and χ_C^{av}. Fig. 3 reports the means and standard deviations of η^{av}, λ^{av}, χ_C^{av}. Fig. 4 does the same for Y_i^{av}. As to WSP, results were taken from [61].

When observing Fig. 2, Fig. 3, and Fig. 4, it should be taken into account that the inlet devolatilization gas was anoxic and dry (N_2 is the only fed gas), so the primary sources of oxygen were the bed material, when OCs were used, and biomass itself.

For all bed materials and biomasses, the temperature change from 700 °C to 900 °C made η^{av}, λ^{av}, and χ_C^{av} increase (Fig. 2 and Fig. 3). This trend agrees with a typical gasification process [87] and other experiments dealing with the devolatilization/gasification of biomass [46,88,89]. The trend of λ^{av} agreed with the behavior of Y_{H2}^{av} and Y_{CO}^{av} (Fig. 4): Y_{H2}^{av} substantially grew as the devolatilization temperature was increased (ranging within 10–23 mol% dry, dilution-free at 700 °C vs. 33–45 mol% dry, dilution-free at 900 °C, see Appendix A); Y_{CO}^{av} was more weakly influenced (ranging within 29–40 mol% dry, dilution-free at 700 °C vs. 35–41 mol% dry, dilution-free at 900 °C, see Appendix A). It is worth observing that the substantial increase of Y_{H2}^{av} always occurred at the expense of the abundance of CO_2, CH_4, and other hydrocarbons as the temperature was increased (Fig. 4), suggesting the enhancement of endothermic reforming reactions, thermodynamically favored by higher temperatures.

Regarding the effects of pretreatments, the values of χ_C^{av} for WSP were generally higher than those of all pretreated biomasses (Fig. 2 and Fig. 3). This could be sensibly ascribed to torrefaction, which is a pretreatment of all studied biomass samples except WSP (Table 1): torrefaction causes the preliminary separation of light volatile matter and leaves in the solid biomass the most recalcitrant carbon towards thermal conversions [46], i.e., it makes shift the properties of biomass towards those of coal [90]. The water-washing did not induce systematic variations of χ_C^{av} as substantial as those that emerged in the comparison between WSP and pretreated biomasses (see Fig. 2 and Fig. 3, e.g., at 900 °C with SIB, WSP had χ_C^{av} = 82.2 %, WSP-T3add had χ_C^{av} = 53.9 %, WSP-T3Wadd had χ_C^{av} = 49.7%). Concerning λ^{av} (Fig. 2 and Fig. 3), the pretreated biomasses developed higher values in comparison to WSP in the vast majority of cases (68 out of 72, see Appendix A); noteworthy, Y_{H2}^{av} of WSP was always the lowest for a given "bed material/temperature" couple (Fig. 4, also see Appendix A). This matches well with results from Chen et al. [91], who experimentally found that carbonaceous gases (CO_2 and CO) are more easily released than H_2 during the preliminary torrefaction pretreatment. Other substantial differences due to pretreatments of wheat straw

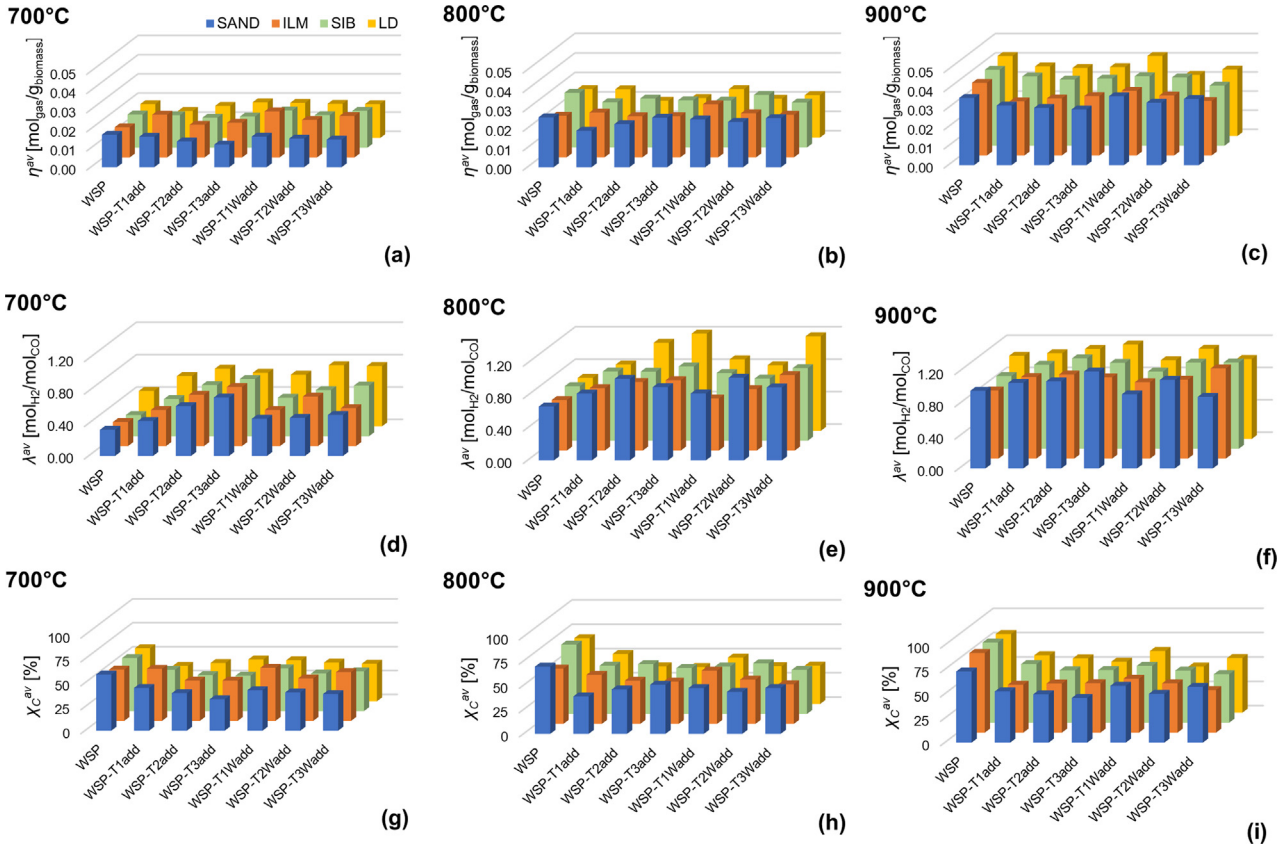

Fig. 2. Experimental results of devolatilization tests (N_2 as fluidizing agent at 1.5 times the minimum fluidization velocity) for all biomasses as functions of devolatilization temperature. Integral-average gas yield η^{av} (Equation 1) (a), (b), (c). Integral-average H_2/CO molar ratio λ^{av} (Equation 2) (d), (e), (f). Integral-average carbon conversion χ_C^{av} (Equation 3) (g), (h), (i). Legend in (a) is valid for the whole Figure. WSP data. adapted from [61]

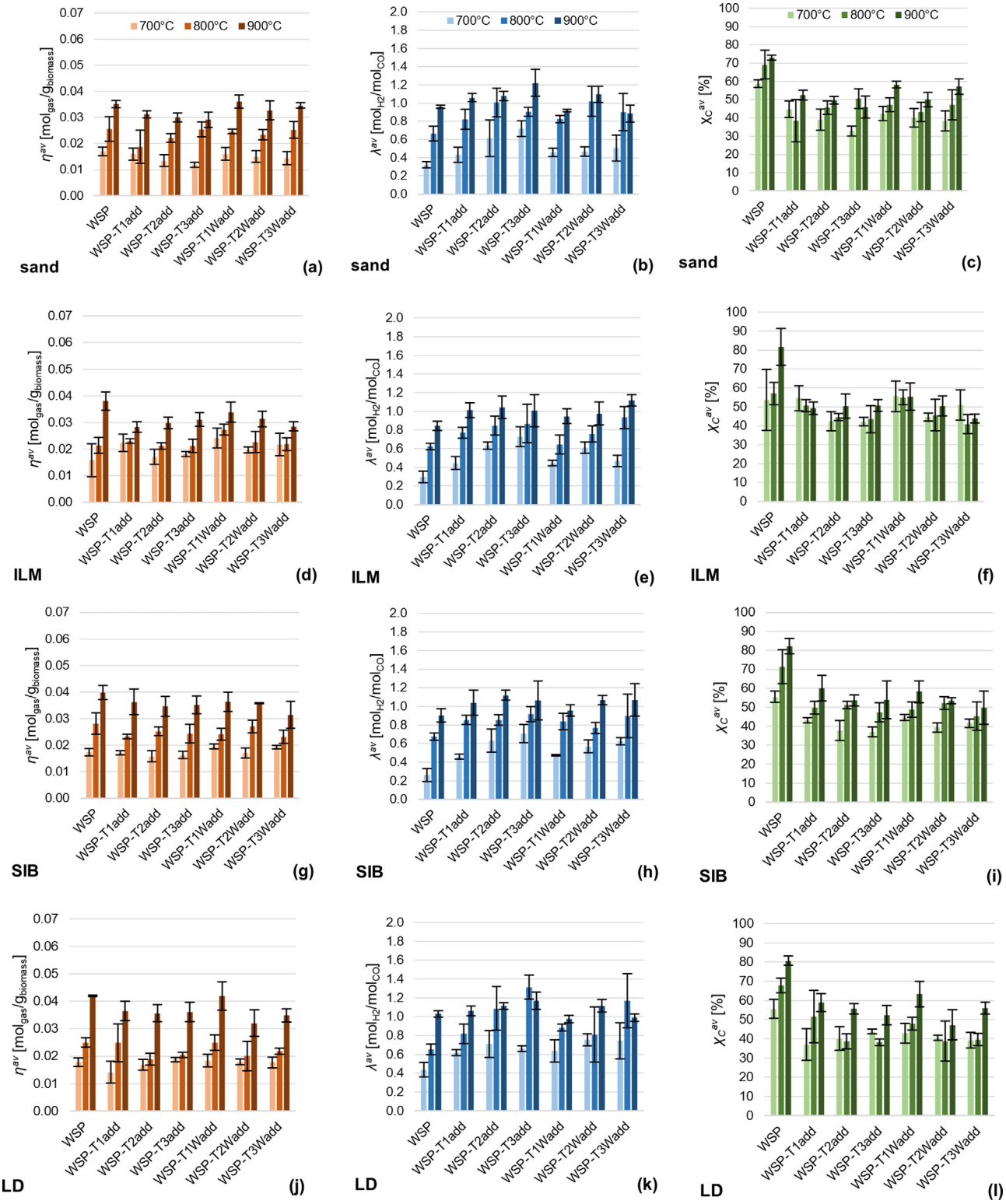

Fig. 3. Experimental results of devolatilization tests (N_2 as fluidizing agent at 1.5 times the minimum fluidization velocity) as functions of devolatilization temperature, kind of biomass, kind of bed material: integral-average gas yield η^{av} (Equation 1) from tests with sand (a) with legend, ILM (d), SIB (g), LD (j); integral-average H_2/CO molar ratio λ^{av} (Equation 2) from tests with sand (b) with legend, ILM (e), SIB (h), LD (k); integral-average carbon conversion χ_C^{av} (Equation 3) from tests with sand (c) with legend, ILM (f), SIB (i), LD (l). Bars height equals arithmetic means out of three experimental replications and error bars the related standard deviations. WSP data . adapted from [61]

were not inferable, net of associated standard deviations (see Appendix A).

Observations and results similar to those discussed so far were obtained from devolatilizations of wheat straw pellets pretreated by torrefaction and water-washing, without the $CaCO_3$ addition by 2 wt% [41,43,44,61]: one can infer that the addition of 2 wt% $CaCO_3$ does not substantially affect the pyrolytic behavior of wheat straw pellets, as done – for instance – by torrefaction.

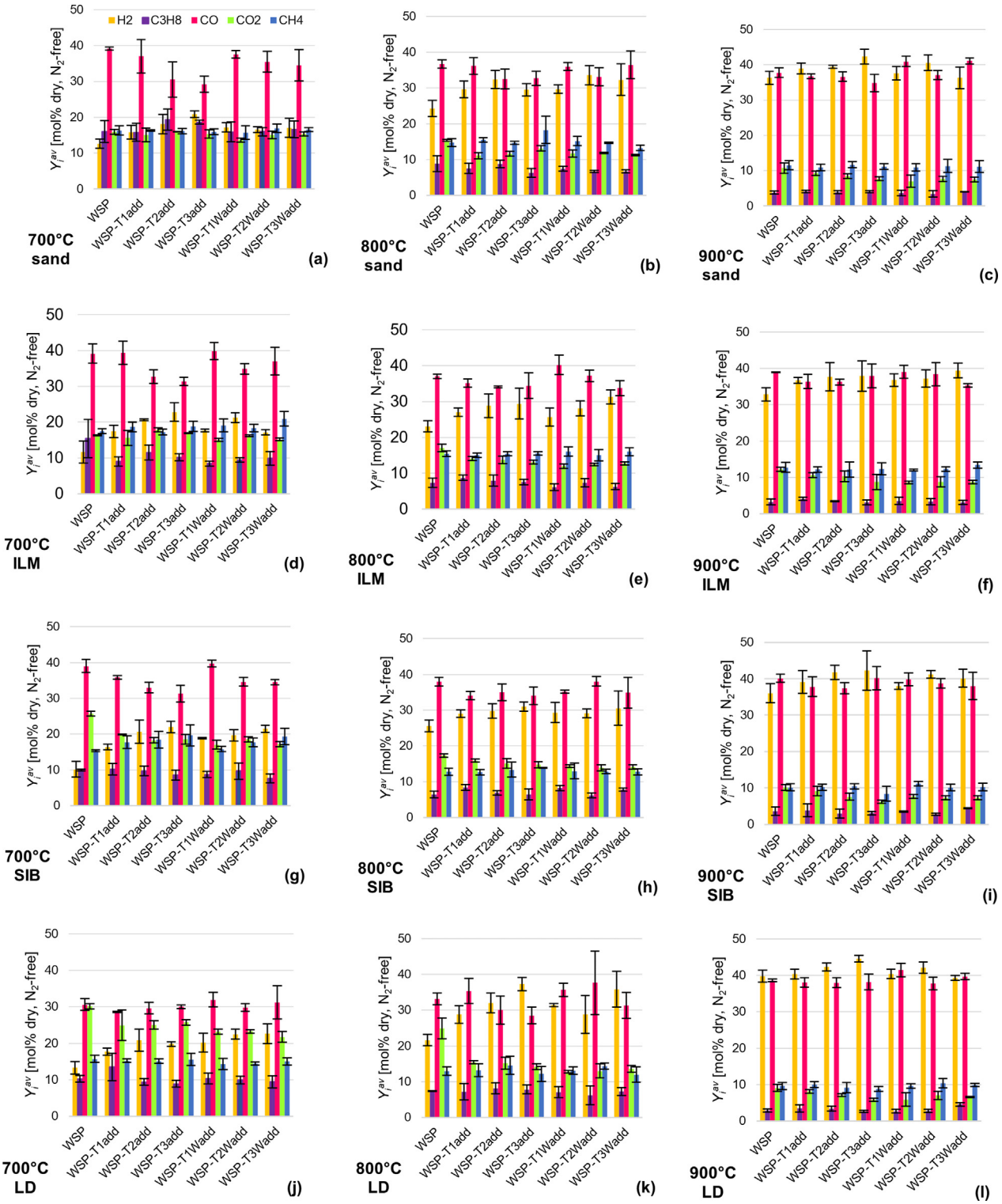

Fig. 4. Experimental integral-average compositions of syngas from devolatilization tests (N_2 as fluidizing agent at 1.5 times the minimum fluidization velocity), as functions of temperature, kind of biomass, kind of bed material, expressed as mol% dry and dilution-free, Y_i^{av} (Equation 4): sand at 700 °C (a), 800 °C (b), 900 °C (c); ILM at 700 °C (d), 800 °C (e), 900 °C (f); SIB at 700 °C (g), 800 °C (h), 900 °C (i); LD at 700 °C (j), 800 °C (k), 900 °C (l). Bars height equals arithmetic means out of three experimental replications and error bars the related standard deviations. Legend in (a) is valid for the whole Figure. WSP data. adapted from [61]

Not-so-clear-cut trends were always observed when considering the influences from the bed material, within the frame of experimental accuracy of proposed devolatilization tests. Anyway, some noteworthy combinations emerged in Fig. 2 and Fig. 3: (i) at 700 °C, ILM with some pretreated biomasses (WSP-T1add, WSP-T1Wadd, WSP-T3Wadd) gave noticeable gas yield and carbon conversion, with the best performance belonging to ILM with WSP-T1Wadd (η^{av} = 0.027 mol_{gas} $g_{biomass}^{-1}$, χ_C^{av} = 54.9 %); (ii) at 900 °C the highest values were obtained with LD (e.g., the best performance at 900 °C was that of LD and WSP-T1Wadd with

η^{av} = 0.042 mol_{gas} $g^{-1}_{biomass}$ χ_C^{av} = 50.6 %). As to those combinations, it is interesting to observe that they always involve pretreated pellets.

In general, all kinds of wheat straw pellets investigated in this work (Table 1) provided pyrolytic performances (Fig. 2, Fig. 3, Fig. 4) comparable with those of pellets of raw pine residues tested at the very same conditions and with the same OCs [61]; this is a useful piece of information for CLG development, since the pine based material can be considered as the closest to current commercial woody pellets [92].

3.2. Pressure fluctuation tests and characterizations after-tests

The experimental conditions to acquire pressure fluctuation signals (see Section 2.4) include a substantial exposure of OCs to ashes (10 vol%) for 30–60 min at each temperature dwell in the range 700–1000 °C. This exposure duration is reasonably lower than the lifetime of the bed inventory in a hypothetical industrial dual interconnected fluidized bed for CLG, so the behavioral tendencies found by this laboratory-scale experimental campaign may be even more influential in actual productive campaigns.

Fig. 5 provides examples of typical cases in the assessment of bubbling fluidization quality, taken from the experimental campaign presented in this work (ILM mixed with ash from WSP-T1Wadd, at $u = 2u_{mf}$): Fig. 5(a) and Fig. 5(c) show pressure fluctuation signals of bubbling beds, Fig. 5(b) and Fig. 5(d) the respective PSDFs with bell-like profiles of locally dominant frequencies, roughly centered between 1 and 10 Hz; Fig. 5(g) shows the typical signal of not-bubbling bed (no fluctuations), corroborated by the absence in its PSDF (Fig. 5(h)) of dominant frequencies sufficiently far from 0 Hz (the limit of aperiodic phenomena); Fig. 5(e) and Fig. 5(f) represent an intermediate situation, with a barely bubbling bed (incipient or fading bubbles).

It is essential to remind that OCs fresh samples belong to generalized Geldart group B at tested conditions (see Section 2.2), so only bubbling fluidization is possible, in principle, at the superficial velocities operated in discussed tests (two and threefold u_{mf}). When observing Fig. 5, it should also be considered that in bubbling fluidized beds, at a given excess velocity (u - u_{mf}), $\sigma_{\Delta P}$ usually increases up to a maximum when the temperature is increased from ambient conditions, then the further increase of temperature determines the decrease of $\sigma_{\Delta P}$ [93]. The progression from Fig. 5(a) to Fig. 5(c) can then fit into the usual behavior of bubbling beds at high temperatures. On the other hand, the disappearing of locally dominant frequency in the PSDFs of Fig. 5(h) is more clearly ascribable to the absence of bubbles.

Due to a large number of acquired fluctuation signals, the assessment of fluidization quality was presented in the

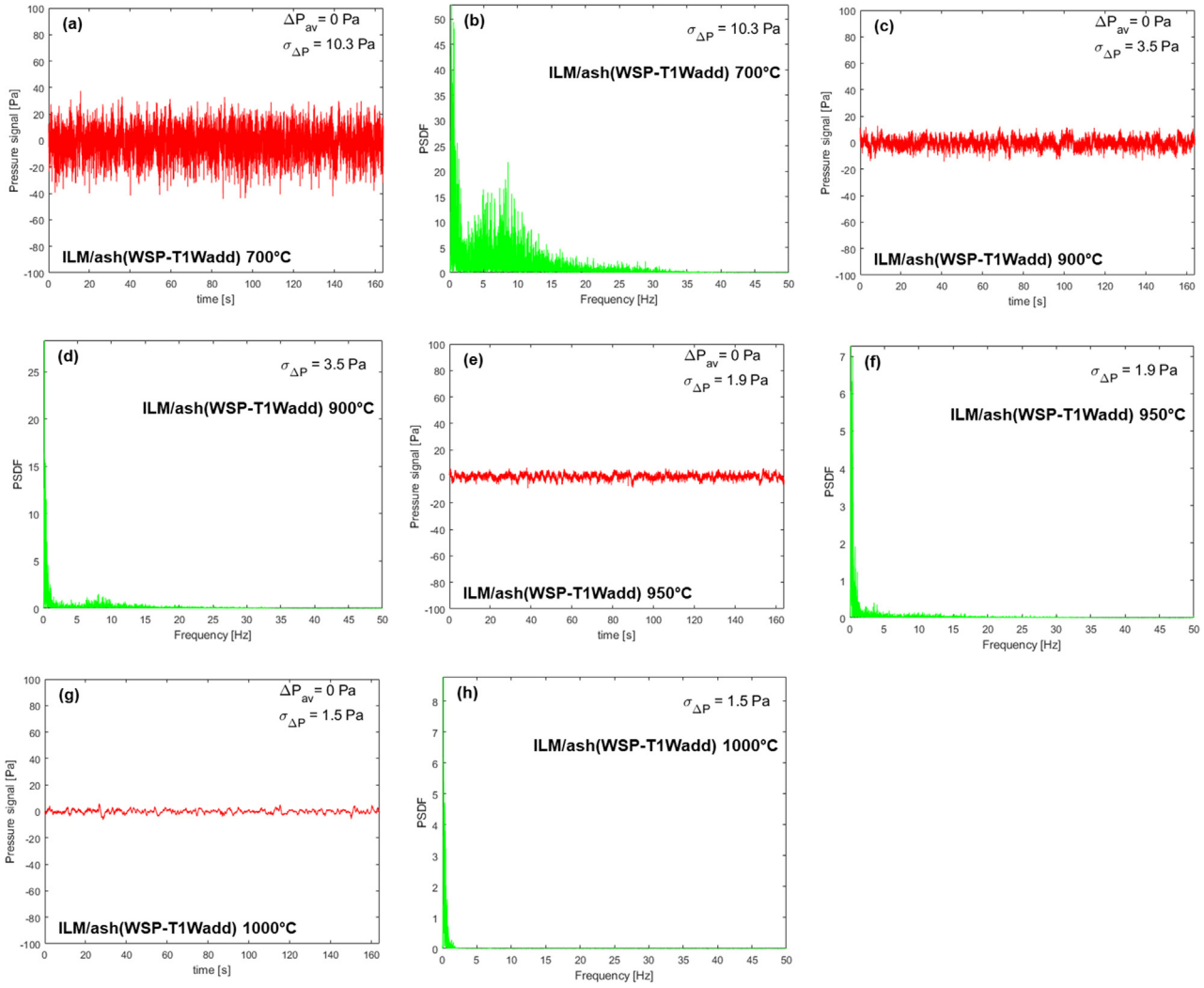

Fig. 5. Pressure fluctuation signals (LHS column) with related PSDFs (RHS column), from the bed made of ILM and ash from WSP-T1Wadd (ILM/ash(WSP-T1add)), fluidized with N_2 at $u = 2u_{mf}$: 700 °C (a), (b); 900 °C (c), (d); 950 °C (e), (f); 1000 °C (g), (h).

summarized form in Fig. 6, where the evaluations criteria just explained regarding Fig. 5 were applied to all tested OC/ash mixings: a green box means that the related pressure fluctuation signal and PSDF represent a well-developed bubbling bed (similarly to Fig. 5(a,b,c,d)); a red box that the related pressure fluctuations and PSDF represent a not-bubbling bed (similarly to Fig. 5(g,h)); a yellow box indicates an intermediate situation (similarly to Fig. 5(e,f)); a white box indicates a not acquired signal.

The summaries in Fig. 6 turned out to be a valuable tool for an overall choice of the most reliable OCs in terms of bubbling fluidization quality at relevant temperatures for CLG. Indeed, no biomass had ashes which outstandingly ensured the best performance independently on the OC.

Whatever the mixed ash, LD had the worst bubbling fluidization quality at both $2u_{mf}$ (Fig. 6(e)) and $3u_{mf}$ (Fig. 6(f)). When LD performances were compared with those of ILM (Fig. 6(a,b)) or SIB (Fig. 6(c,d)), the fading out of bubbling fluidization always occurred at lower temperatures.

At the lowest superficial velocity ($2u_{mf}$) with ILM (Fig. 6(a)) and SIB (Fig. 6(c)), some positive effects of pretreatments emerged, as ashes of pretreated biomasses frequently delayed to higher temperatures the insurgence of defluidization, in comparison to homologous tests with WSP ash (showy exceptions occurred for WSP-T3add ash with ILM and WSP-T2Wadd with SIB).

The increase up to $3u_{mf}$ generally improved the bubbling fluidization quality with all three OCs (Fig. 6(b,d,f)) and, in many cases, it brought back to the bubbling regime beds without bubbles at $2u_{mf}$ (Fig. 6(a,c,e)). This was an important indication for the operation of CLG at demonstrative or commercial scales with dual interconnected fluidized beds, for sure operated at superficial velocities higher than $3u_{mf}$: the OCs and ashes studied in this work could recover bubbling fluidization by the increase of superficial velocities. It is worth stressing that the chosen laboratory-scale operating conditions may be more detrimental than those of the actual CLG demonstrative/commercial operations: low exerted u ($\leq 3u_{mf}$) and substantial presence of ashes (10 vol% in the bed) disfavored the separation of the latter from OC particles (e.g., ash particles segregation or elutriation); actual demonstrative/commercial CLG conditions (i.e., higher u and lower ash accumulation in the bed) could prevent or limit the negative ash/OC interactions.

The qualitative evaluations obtained from the analysis of pressure fluctuation signals (Fig. 6) found coherent corroboration in the results of characterizations by SEM-EDS and PSDs of OC/ash mixings after fluidizations at high temperatures.

Samples from mixed beds of OC/ash in Fig. 6 were observed by SEM and analyzed by EDS. The examples of SEM micrographs in Fig. 7 and SEM-EDS maps in Fig. 8 were descriptive of generally observed phenomena. Modifications detected by SEM-EDS were ascribable to the intrinsic nature of the OCs, rather than to the behavior of a given ash at high temperature. It is worth noting that all three OCs contained themselves some of the elements typically responsible for agglomeration issues, generally contained in ashes (e.g., Si and K found by characterizations of fresh OCs in [6,41]). This evidence may partially nullify the beneficial effects of biomass water-washing on the prevention of agglomeration, such as the K removal [6].

As to ILM, inferences from SEM-EDS observations revealed good stability of the chemical composition and particle dimensions (d_p of fresh ILM was 255 μm [6]), together with a low predisposition towards agglomeration (Fig. 7(a,b)); the compresence of K (sensibly due to ash) and Ti (from ILM) in the same zones (Fig. 8(a)) is in agreement with Hildor et al. [80] who found K-titanates in their chemical-looping experiments with ilmenite.

Samples of SIB at 1000 °C systematically presented agglomeration, independently of the kind of coupled ash (e.g., Fig. 7(c,d)). SEM-EDS (Fig. 8(b)) explained this agglomeration tendency: it is worth knowing that fresh SIB contained some traces of Pb [6], which turned out to be chemically unstable during the fluidization at high temperature, acting synergistically with low-melting elements such as Si and K to form bridges that worked as an agglomeration center of SIB particles (see the combined presence of Pb, Si, and K in Fig. 8(b)). Since the d_p of fresh SIB was 208 μm [6], Fig. 7(c, d) and Fig. 8(b) suggested that the agglomeration by Pb-based bridges mainly involved small SIB fragments.

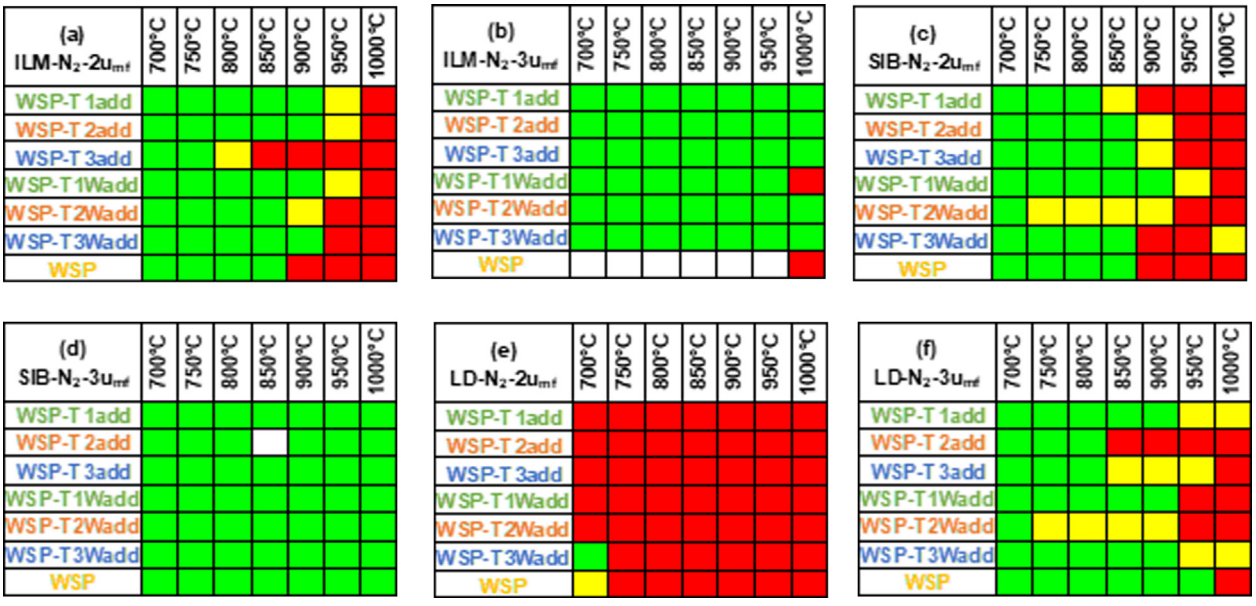

Fig. 6. Evaluation of the fluidization quality, based on experimental pressure fluctuation signals, their standard deviation, and locally dominant frequencies in PSDFs; beds made up of OCs mixed with ashes from WSP, torrefied and torrefied-washed biomasses, both with mineral additives; Legend: green = bubbling bed; yellow = bubbling fluidization fading out; red = no bubbling; and white = acquisition missed. (For interpretation of the references to colour in this figure legend, the reader is referred to the web version of this article.)

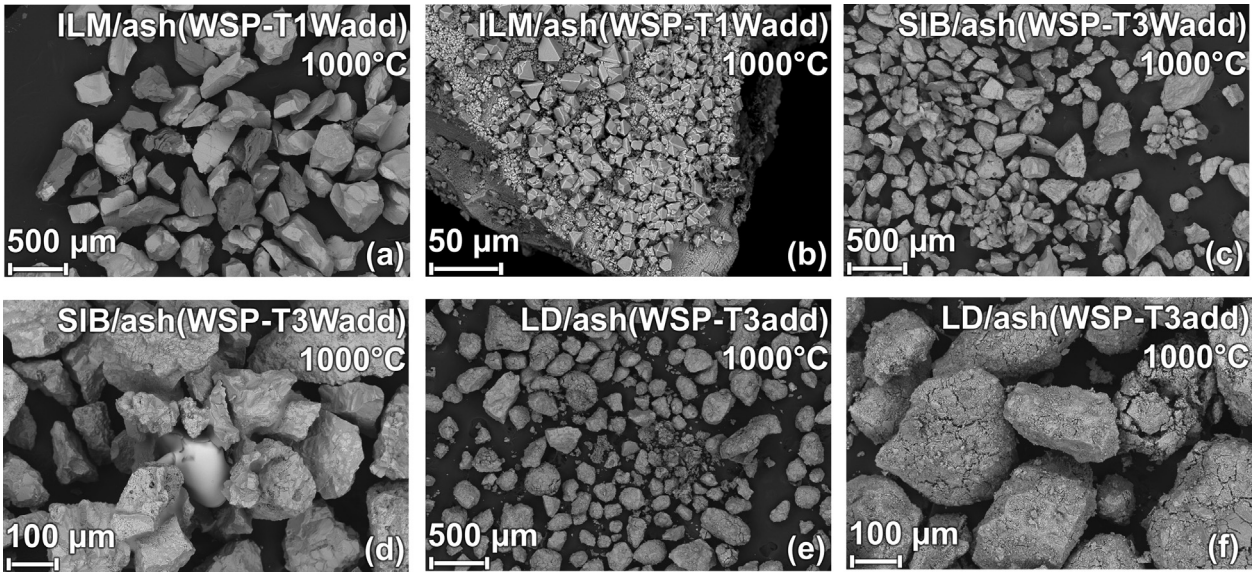

Fig. 7. Bed samples after fluidizations with N_2 up to $3u_{mf}$ and 1000 °C: ILM with ashes of WSP-T1Wadd (80× (a) and 1000× (b)); SIB with ashes of WSP-T3Wadd (80× (c) and 350× (d)); LD with ashes of WSP-T3add (80× (e) and 350× (f)).

LD particles did not agglomerate, but a severe fragmentation occurred, forming fines with diameters lower than 100 µm (d_p of fresh LD was 235 µm [6]), especially after treatments at 1000 °C (Fig. 7(e,f)).

The diffused presence of P in samples of SIB (Fig. 8(b)) and LD (Fig. 8(c)) suggested an interaction with ashes, since P was absent in fresh OC samples but present in the wheat straw ashes, so working as an "ash tracer".

Treatments in bubbling fluidized beds up to 1000 °C with ashes engendered different modifications of the OCs' d_p (Table 2) and PSDs (Fig. 9).

As to ILM and SIB, ashes from WSP caused the highest increase of d_p (see percentage variations Δd_p in Table 2), i.e., pretreatments improved the ash behavior of wheat straw pellets as far as the limitation of agglomeration is concerned. Regarding LD, the results are substantially different since all after-test samples underwent an important decrease of d_p (Table 2), confirming the quantitative significance of the cracking observed by SEM (Fig. 7(e,f)).

Values of d_p in Table 2 for LD made the bed inventories approach or cross the border between Group B and Group A (homogeneous fluidization) in the generalized Geldart map by Gibilaro [34], at the chosen fluidization conditions (1000 °C with N_2 as the fluidizing agent). For Geldart group A particles, the superficial velocity of minimum bubbling is higher than that of minimum fluidization, allowing homogeneous fluidization (expanded bed without bubbles) for the superficial velocities between those two thresholds [34].

The positive effect of biomass pretreatments in limiting ILM and SIB agglomeration is also evident in PSDs (Fig. 9(a,b)). For both OCs, the PSD of the bed fluidized at 1000 °C with WSP ashes is the most shifted to the right, compared to the fresh one. The agglomeration tendency of SIB small particles observed by SEM-EDS (Fig. 7(c,d) and Fig. 8(b)) was confirmed by the disappearance of its finest fraction in the fresh sample (red line in the magnification of Fig. 9(b), 10–100 µm). On the other hand, the intrinsic tendency to cracking of the studied LD sample (Fig. 7(e,f) and Fig. 8(c)) overcame the effects of the biomass pretreatments, determining the formation of bimodal PSDs after the fluidization at 1000 °C with ashes (Fig. 9(c)): a second bell of finer particles appeared between 10 and 100 µm (magnification of Fig. 9(c)). Condori et al. [13] successfully used Linz-Donawitz slag for CLG of biomasses in dual interconnected fluidized beds (1.5 kW_{th}), proving its suitability for that process; a preliminary selection of more robust LD particles may solve the fluidization problems faced during the experimentation discussed in this work.

3.3. Overall experimental considerations

The first consideration concerns the straightforwardness of the proposed methodology. The two proposed test campaigns (devolatilizations and pressure fluctuation acquisitions) investigated two critical aspects for developing CLG at higher scales: thermochemical performance and fluid-dynamics. In principle, they could be evaluated by bench-scale fluidized bed gasification tests; still, the time demand would become insurmountable if combinations of many types of biomasses, bed materials and process conditions were to be explored, as in the case of this work. The experimental experiences suggest that a bench-scale fluidized bed gasifier can perform no more than 1–2 tests per week, in the best case; in contrast, the laboratory-scale procedures of this work allowed exploring more than one condition per day. As a matter of fact, those procedures allowed an important screening of feedstock and materials, by providing comparable sets of data for each set of conditions.

As far as the development of CLG technology is concerned, the thermochemical and fluid-dynamic evaluations are preliminary but mandatory steps, even though the final choice of biomasses, pretreatments, and OCs for the full commercial scale also depends on availability, technical and economic convenience, practicability of the pretreatments, logistic of providers, etc.

From an overall point of view, only the combined interpretation of results from devolatilizations and pressure fluctuation acquisitions comprehensively highlighted the different behavioral improvements due to the introduction of novel pretreatments on wheat straw pellets, such as: (i) the very frequently higher λ^{av} (Fig. 3 and Appendix A) and Y^{av}_{H2} (Fig. 4 and Appendix A) of pretreated pellets compared to WSP, which are key factors for the subsequent synthetic steps that convert syngas, e.g., the catalytic synthesis of biofuels [27,28]; (ii) the general limitation of the increase of d_p for ILM or SIB fluidized with ashes, when compared to effects on d_p due to WSP ash (Fig. 9 and Table 2). In other words, WSP (i.e., untreated wheat straw pellets) emerged as the worst

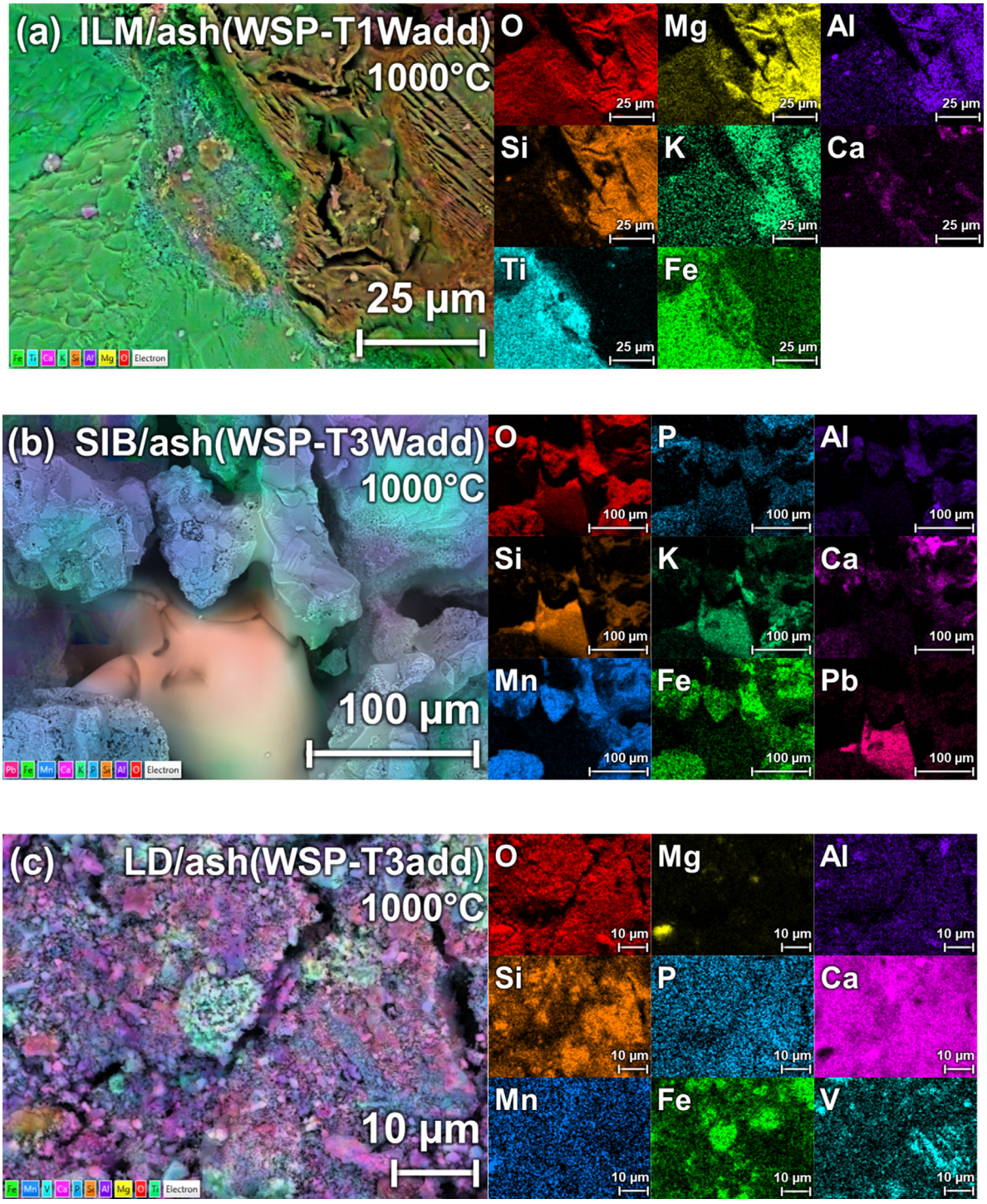

Fig. 8. ILM mixed with ashes from WSP-T3Wadd fluidized in N_2 up to $3u_{mf}$ and 1000 °C at 3000x with segregated elements (a); SIB mixed with ashes from WSP-T3Wadd fluidized in N_2 up to $3u_{mf}$ and 1000 °C at 1000x with segregated elements (b); LD mixed with ashes from WSP-T3add fluidized in N_2 up to $3u_{mf}$ and 1000 °C at 5000x with segregated elements (c).

choice to develop CLG at higher scales. These are important indications for those researchers interested in exploiting lignocellulosic biomasses, sustaining the need for pretreatments to improve both thermochemical and fluid-dynamic aspects of their conversion processes in fluidized bed facilities.

The nature of OCs was crucial to the bubbling fluidization quality. The three OCs themselves contained some of the low-melting elements that were targets of the washing pretreatment removal, such as alkali and alkali earths metals [6]. In other words, one of the reasons of biomass water-washing may decay; on the other hand, the water-washing was proved to be a desulfurizing pretreatment for biomasses [6], an issue not considered by the quantifications of this work.

Lebendig et al. [75] investigated the same biomasses with $CaCO_3$ addition and the same OCs of this work by both experimental and thermodynamic-modeling tools, with a specific focus on the behavior of biomass ashes as an agglomeration trigger. They [75] concluded that the addition of $CaCO_3$ combined with

Table 2
Particle average diameters (d_p) of OCs mixed with ashes from biomasses after pressure fluctuation tests with N_2 up to $3u_{mf}$ and 1000 °C; percentage d_p variation of after-test samples (Δd_p), with OCs particle diameter in the fresh state as a reference.

Biomass ash	ILM		SIB		LD	
	d_p (μm)	Δd_p (%)	d_p (μm)	Δd_p (%)	d_p (μm)	Δd_p (%)
WSP	290	+14	260	+25	137	−42
WSP-T1add	265	+4	242	+16	125	−47
WSP-T3add	249	−2	226	+9	58	−75
WSP-T1Wadd	253	−1	217	+5	95	−59
WSP-T3Wadd	257	+1	192	−8	77	−67

torrefaction and torrefaction-washing is adequate to limit the formation of slags and low melting systems. This was confirmed by the results in Table 2 for ILM and SIB; on the other hand, the peculiar mechanical effects of fluidization on LD particles and their consequences on fluidization quality were out of the range of phenomena considered by Lebendig et al. [75], as well as the critical effects due to the traces of Pb in SIB. On the other hand, Lebendig et al. [75] experimentally and thermodynamically considered the release of pollutants in the gas phase (e.g., compounds of sulfur, alkali, chlorine, and phosphorous), in relation to the different pretreatments of ashes; this is a relevant aspect to CLG, but beyond the subject in the present study.

Overall, when considering the fluid-dynamic conditions of the CLG process, ILM appeared as the most stable OC. Peculiar Pb traces of SIB favored its agglomeration, independently of the interacting ash (Fig. 8(b,c), Fig. 9(b)). LD fragility jeopardized the bubbling fluidization quality under tested conditions (Fig. 6).

Together, the two experimentations allowed the selection of pretreated wheat straw biomasses and ILM as the most promising materials for CLG experimentations at higher scales. Further details on pretreatments also need to be delineated by evaluating feasibility and costs at higher scales; in fact, the considered process variables did not always show significant trends within the frame of experimental accuracy when the different pretreatments are considered.

4. Conclusions

Pretreated wheat straw pellets (torrefied with added 2 wt% $CaCO_3$, optionally water-washed) and three oxygen carriers (ilmenite, calcined "Sibelco", Linz-Donawitz slag) were investigated under the aegis of the ongoing Horizon2020 project CLARA, currently the only European research project dealing with chemical looping gasification for II generation biofuels, up to the MW_{th}-scale.

The two proposed methodologies (pellet devolatilizations and pressure fluctuation acquisitions) – based on laboratory-scale fluidized beds – proved to be a new, straightforward, but rigorous tool to select oxygen carriers and solid fuels eligible for further investigation of chemical looping gasification at higher scales, among the numerous possible bed material/biomass combinations.

As to thermochemical aspects (devolatilizations):

- Whatever the investigated biomass or bed material, the increase of devolatilization temperature from 700 °C to 900 °C made increase syngas yield, H_2/CO ratio, biomass carbon conversion, and the H_2 content in syngas (10–23 mol% dry, dilution-free at 700 °C vs. 33–45 mol% dry, dilution-free at 900 °C), thanks to the conversion of gaseous hydrocarbons.
- Pretreated pellets generally involved higher H_2/CO ratios in devolatilized syngas and lower carbon conversion in the biomass; this was ascribed to torrefaction.
- The addition of 2 wt% of $CaCO_3$ as a wheat straw pretreatment did not affect devolatilization performances, within the frame of experimental accuracy.

As to assessment of bubbling fluidization (pressure fluctuation acquisitions from oxygen carrier/ash mixed beds accompanied by SEM-EDS and measurements of particle size distributions):

- ilmenite was the most chemically and mechanically stable material, compared to calcined "Sibelco" and Linz-Donawitz slag, as it ensured good bubbling fluidization quality with no severe fragmentation/comminution or agglomeration in the presence of wheat straw ashes.
- Studied biomass pretreatments (torrefaction and 2 wt% $CaCO_3$ addition, optional water-washing) limited or prevented the increase of particle diameters of ilmenite, having as a reference the effects from ashes of raw wheat straw pellets.

Ilmenite is the most promising oxygen carrier (compared to calcined "Sibelco" and Linz-Donawitz slag) and pretreated wheat straw pellets are more suitable than pellets of raw wheat straw for further studies about chemical looping gasification at demonstration scales to be carried out for the first time.

5. Symbols and abbreviations

$\%ash_{db}$ – biomass ash content, wt% on a dry basis (db).
$\%C_{daf}$ – elemental carbon in biomass, wt% on a dry ash-free basis (daf).
$\%moisture_{ar}$ – biomass moisture content, wt% as received (ar).
d_p – particle diameter, μm.
$F_{i,out}$ – outlet molar flow rate of gaseous component i, mol min^{-1}.
m_p – mass of the pellet, g.
n_j – number of carbon atoms in the component j, dimensionless.
t – devolatilization time, min.
u – superficial gas velocity, cm s^{-1}.
u_{mf} – minimum fluidization velocity, cm s^{-1}.
Y_i^{av} – integral-average (av) molar fraction of gaseous component i, mol% dry, dilution-free.
χ_C^{av} – integral-average (av) carbon conversion, %.
Δd_p – percentage particle diameter variation, %.
η^{av} – integral-average (av) gas yield, $mol_{gas}\ g_{biomass}^{-1}$.
λ^{av} – integral-average (av) H_2/CO molar ratio, $mol_{H2}\ mol_{CO}^{-1}$.
$\sigma_{\Delta P}$ – standard deviation of pressure fluctuation signals, Pa.
ar – as received.
av – integral-average.
daf – dry, ash-free.
db – dry basis.
BECCS – BioEnergy with Carbon Capture and Storage.
CCS – Carbon Capture and Storage.
CENER – Centro Nacional de Energías Renovables.

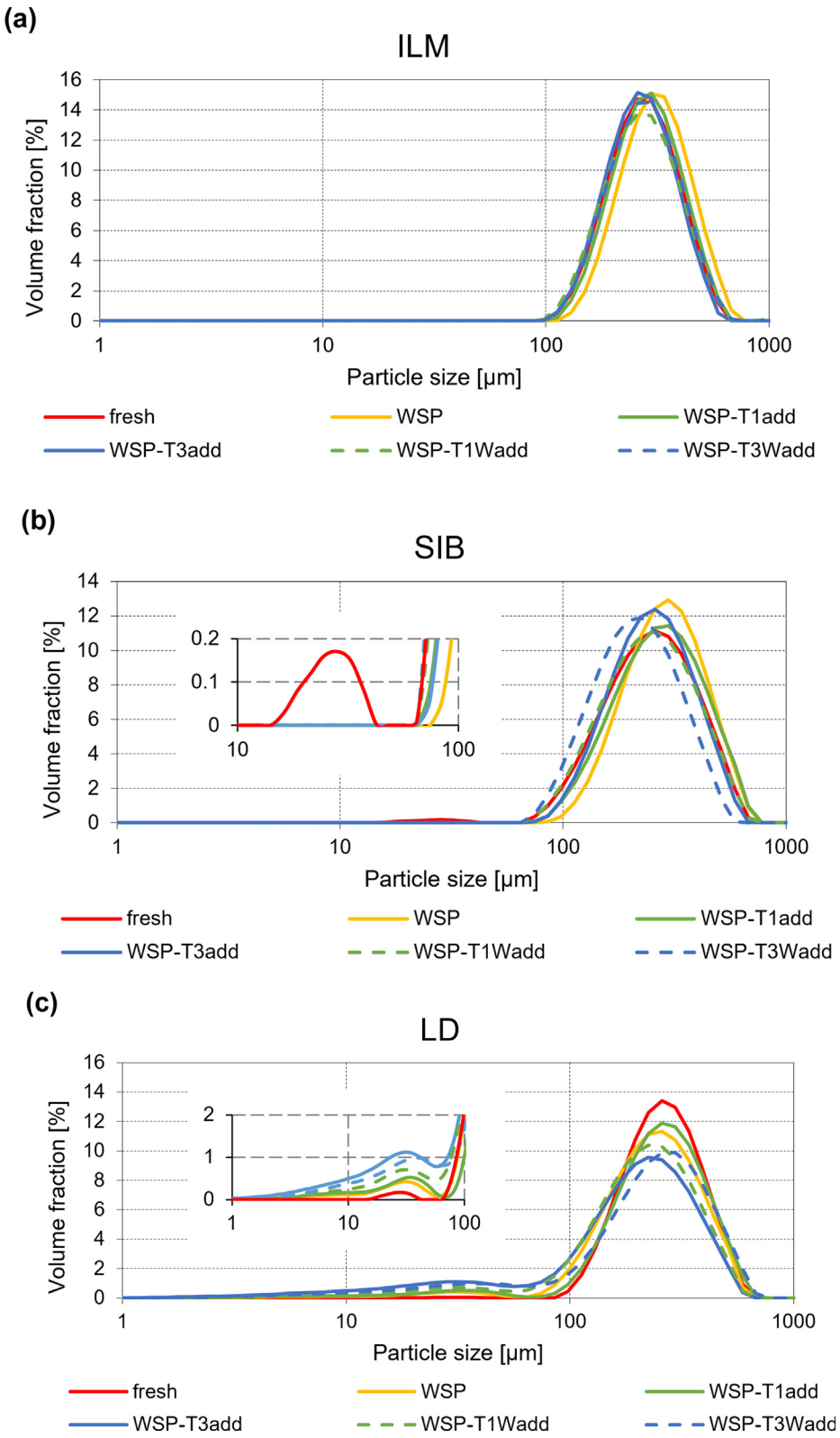

Fig. 9. Comparisons of OCs Particle Size Distributions (PSDs), in the fresh state and mixed with ashes from WSP, WSP-T1add, WSP-T3add, WSP-T1Wadd, and WSP-T3Wadd after pressure fluctuation acquisitions in beds fluidized with N_2 up to $3u_{mf}$ and 1000 °C: ILM (a); SIB (b); LD (c).

CLARA – Chemical Looping gAsification foR sustAinable production of biofuels.

CLG – Chemical Looping Gasification.

EDS – Energy Dispersion X-ray Spectrometry.

ILM – ilmenite OC.

IPCC – United Nations Intergovernmental Panel on Climate Change.

LD – Linz-Donawitz-slag OC.

LHS – Left Hand Side.
NET – Negative Emissions Technologies.
OC – Oxygen Carrier.
PSD – Particle Size Distribution.
PSDF – Power Spectral Density Function.
RHS – Right Hand Side.
SEM – Scanning Electron Microscopy.
SIB – calcined "Sibelco" OC.
WSP – Wheat Straw Pellet (see Table 1).
WSP-T*x*add – Wheat Straw Pellet-Torrefied at temperature "T*x*" (T1 = 250 °C, T2 = 260 °C, or T3 = 270 °C)), with 2 wt% $CaCO_3$ (see Table 1).
WSP-T*x*Wadd – Wheat Straw Pellet-Torrefied at temperature "T*x*" (T1 = 250 °C, T2 = 260 °C, or T3 = 270 °C)) and Washed, with 2 wt% $CaCO_3$ (see Table 1).

CRediT authorship contribution statement

Andrea Di Giuliano: Conceptualization, Methodology, Software, Validation, Formal analysis, Investigation, Data curation, Writing – original draft, Writing – review & editing, Visualization, Supervision. **Barbara Malsegna:** Software, Investigation, Data curation. **Stefania Lucantonio:** Software, Investigation, Data curation, Visualization. **Katia Gallucci:** Conceptualization, Methodology, Validation, Formal analysis, Investigation, Resources, Data curation, Writing – review & editing, Supervision, Project administration, Funding acquisition.

Declaration of Competing Interest

The authors declare that they have no known competing financial interests or personal relationships that could have appeared to influence the work reported in this paper.

Acknowledgements

This research and the APC were funded by the Horizon 2020 Framework program of the European Union, CLARA project, G.A. 817841.

The authors warmly thank Giampaolo Antonelli for PSD measurements, Lorenzo Arrizza and Maria Giammatteo for SEM-EDS management, and Leonardo Zennaro for his assistance in pressure fluctuation experiments.

The production and characterization of biomass pellets by the research team of the National Renewable Energy Centre of Spain (CENER) is acknowledged, as well as the provision of oxygen carriers by the University of Chalmers (Sweden), and the mineral additives by Forschungszentrum Jülich GmbH (Germany), all occurred within the CLARA project.

Appendix A. Numerical values of devolatilizations results

See Tables A1–A4.

Table A1
Results from devolatilization tests with sand ("Mean" = arithmetic mean out of the three experimental replications; "St.dev." = standard deviation out of the three experimental replications).

Sand 700 °C	η^{av} [mol/g biomass]		λ^{av} [mol/mol]		χ_C^{av} [%]		Y_{H2}^{av} [vol% dry dil.-free]		Y_{C3H8}^{av} [vol% dry dil.-free]		Y_{CO}^{av} [vol% dry dil.-free]		Y_{CO2}^{av} [vol% dry dil.-free]		Y_{CH4}^{av} [vol% dry dil.-free]	
	Mean	St.dev.	Mean	St.dev.	Mean	St.dev.	Mean	St.dev.	Mean	St.dev.	Mean	St.dev.	Mean	St.dev.	Mean	St.dev.
WSP	0.0169	0.002	0.322	0.035	58.81	2.134	12.58	1.281	16.03	3.072	39.15	0.422	15.94	0.704	16.30	1.316
WSP–T1add	0.0160	0.002	0.432	0.084	44.70	4.497	15.79	1.913	15.77	2.526	37.06	4.692	15.08	1.962	16.31	0.237
WSP–T2add	0.0134	0.002	0.614	0.201	39.16	5.742	18.09	2.652	19.32	3.006	30.52	4.879	15.95	0.070	16.12	0.695
WSP–T3add	0.0118	0.001	0.720	0.085	32.84	2.616	20.89	0.942	18.63	0.587	29.20	2.304	15.35	1.137	15.93	0.804
WSP–T1Wadd	0.0160	0.002	0.458	0.046	42.37	3.974	17.20	1.273	15.92	2.800	37.59	1.074	13.62	0.587	15.67	1.928
WSP–T2Wadd	0.0150	0.002	0.469	0.052	40.02	5.056	16.55	0.809	15.96	1.144	35.48	2.838	15.09	1.076	16.92	1.201
WSP–T3Wadd	0.0144	0.002	0.505	0.145	38.35	5.621	17.02	2.620	16.61	2.334	34.50	4.337	15.29	0.540	16.59	0.541
Sand 800 °C	η^{av} [mol/g biomass]		λ^{av} [mol/mol]		χ_C^{av} [%]		Y_{H2}^{av} [vol% dry dil.-free]		Y_{C3H8}^{av} [vol% dry dil.-free]		Y_{CO}^{av} [vol% dry dil.-free]		Y_{CO2}^{av} [vol% dry dil.-free]		Y_{CH4}^{av} [vol% dry dil.-free]	
	Mean	St.dev.	Mean	St.dev.	Mean	St.dev.	Mean	St.dev.	Mean	St.dev.	Mean	St.dev.	Mean	St.dev.	Mean	St.dev.
WSP	0.0256	0.005	0.664	0.082	69.16	7.787	24.31	2.286	8.86	2.171	36.72	1.194	15.35	0.286	14.75	1.050
WSP–T1add	0.0188	0.006	0.824	0.111	38.51	11.608	29.66	2.341	7.57	1.403	36.18	2.322	11.07	0.872	15.53	0.589
WSP–T2add	0.0221	0.002	1.008	0.158	45.70	3.687	32.44	2.517	8.79	1.011	32.48	2.774	11.62	0.666	14.68	0.423
WSP–T3add	0.0255	0.003	0.904	0.049	50.55	5.351	29.53	1.735	6.33	1.229	32.70	1.953	13.14	0.744	18.31	3.798
WSP–T1Wadd	0.0246	0.001	0.825	0.038	47.15	3.766	29.68	1.217	7.45	0.668	35.99	1.091	11.69	0.997	15.20	1.289
WSP–T2Wadd	0.0233	0.002	1.020	0.165	43.26	5.402	33.56	2.685	6.71	0.350	33.18	2.511	11.84	0.162	14.71	0.187
WSP–T3Wadd	0.0252	0.003	0.900	0.204	47.19	8.148	32.31	4.422	6.72	0.393	36.48	3.846	11.23	0.173	13.26	0.750
Sand 900 °C	η^{av} [mol/g biomass]		λ^{av} [mol/mol]		χ_C^{av} [%]		Y_{H2}^{av} [vol% dry dil.-free]		Y_{C3H8}^{av} [vol% dry dil.-free]		Y_{CO}^{av} [vol% dry dil.-free]		Y_{CO2}^{av} [vol% dry dil.-free]		Y_{CH4}^{av} [vol% dry dil.-free]	
	Mean	St.dev.	Mean	St.dev.	Mean	St.dev.	Mean	St.dev.	Mean	St.dev.	Mean	St.dev.	Mean	St.dev.	Mean	St.dev.
WSP	0.0352	0.001	0.961	0.017	72.94	1.350	36.28	1.825	3.75	0.430	37.74	1.334	10.72	1.471	11.51	1.289
WSP–T1add	0.0312	0.001	1.060	0.043	52.48	2.742	38.94	1.522	4.08	0.321	36.75	0.674	9.27	0.643	10.95	0.912
WSP–T2add	0.0300	0.002	1.078	0.049	49.62	2.045	39.43	0.401	3.85	0.441	36.63	1.386	8.43	0.661	11.67	0.852
WSP–T3add	0.0291	0.003	1.222	0.148	45.89	6.057	42.30	2.120	4.05	0.317	34.82	2.499	7.69	0.590	11.14	0.762
WSP–T1Wadd	0.0361	0.003	0.918	0.016	58.29	1.915	37.58	1.945	3.62	0.801	40.94	1.470	6.98	1.731	10.88	1.063
WSP–T2Wadd	0.0326	0.004	1.096	0.087	50.10	3.954	40.57	2.237	3.41	0.877	37.08	1.317	7.65	0.737	11.29	1.835
WSP–T3Wadd	0.0346	0.001	0.885	0.094	57.16	4.091	36.30	3.068	4.02	0.101	41.07	0.905	7.47	0.659	11.14	1.616

Table A2
Results from devolatilization tests with ILM ("Mean" = arithmetic mean out of the three experimental replications; "St.dev." = standard deviation out of the three experimental replications).

ILM 700 °C	η^{av} [mol/g biomass]		λ^{av} [mol/mol]		χ_C^{av} [%]		Y_{H2}^{av} [vol% dry dil.-free]		Y_{C3H8}^{av} [vol% dry dil.-free]		Y_{CO}^{av} [vol% dry dil.-free]		Y_{CO2}^{av} [vol% dry dil.-free]		Y_{CH4}^{av} [vol% dry dil.-free]	
	Mean	St.dev.	Mean	St.dev.	Mean	St.dev.	Mean	St.dev.	Mean	St.dev.	Mean	St.dev.	Mean	St.dev.	Mean	St.dev.
WSP	0.0158	0.006	0.296	0.060	53.62	16.194	11.68	3.067	15.42	5.323	39.11	2.699	16.32	0.142	17.47	0.703
WSP–T1add	0.0223	0.003	0.445	0.068	54.49	6.555	17.41	1.680	9.00	1.328	39.36	3.240	15.59	2.106	18.64	1.355
WSP–T2add	0.0171	0.003	0.632	0.037	42.26	5.081	20.63	0.224	11.53	2.055	32.72	1.941	17.86	0.582	17.27	0.786
WSP–T3add	0.0181	0.001	0.729	0.106	42.17	2.249	22.80	2.558	10.11	0.989	31.39	1.168	16.88	0.111	18.81	1.426
WSP–T1Wadd	0.0241	0.004	0.445	0.028	55.45	8.199	17.67	0.338	8.38	0.698	39.81	2.434	15.05	0.449	19.08	1.749
WSP–T2Wadd	0.0196	0.001	0.610	0.062	44.47	2.123	21.22	1.325	9.40	0.622	34.87	1.473	16.16	0.277	18.36	1.037
WSP–T3Wadd	0.0217	0.004	0.467	0.063	50.94	7.944	17.13	0.727	9.85	1.861	36.98	3.855	15.17	0.357	20.87	2.051
ILM 800 °C	η^{av} [mol/g biomass]		λ^{av} [mol/mol]		χ_C^{av} [%]		Y_{H2}^{av} [vol% dry dil.-free]		Y_{C3H8}^{av} [vol% dry dil.-free]		Y_{CO}^{av} [vol% dry dil.-free]		Y_{CO2}^{av} [vol% dry dil.-free]		Y_{CH4}^{av} [vol% dry dil.-free]	
	Mean	St.dev.	Mean	St.dev.	Mean	St.dev.	Mean	St.dev.	Mean	St.dev.	Mean	St.dev.	Mean	St.dev.	Mean	St.dev.
WSP	0.0214	0.003	0.624	0.035	56.93	5.915	23.11	1.541	7.33	1.286	37.03	0.642	17.04	1.030	15.49	0.795
WSP–T1add	0.0230	0.001	0.770	0.057	50.57	3.205	27.01	1.193	8.72	0.721	35.12	1.123	14.09	0.515	15.06	0.637
WSP–T2add	0.0211	0.001	0.845	0.102	44.53	1.737	28.79	3.271	7.94	1.539	34.07	0.228	13.73	0.988	15.47	0.582
WSP–T3add	0.0212	0.003	0.868	0.207	43.45	7.047	29.39	4.288	7.55	0.744	34.43	3.546	13.12	0.574	15.51	0.456
WSP–T1Wadd	0.0273	0.002	0.643	0.101	54.88	3.942	25.68	2.499	6.10	0.920	40.20	2.706	11.94	0.670	16.08	1.312
WSP–T2Wadd	0.0226	0.004	0.757	0.086	45.55	8.380	28.04	2.081	7.30	1.168	37.15	1.581	12.48	0.360	15.02	1.547
WSP–T3Wadd	0.0219	0.002	0.933	0.116	40.89	4.990	31.26	2.002	6.27	0.851	33.69	2.126	12.74	0.477	16.04	1.093
ILM 900 °C	η^{av} [mol/g biomass]		λ^{av} [mol/mol]		χ_C^{av} [%]		Y_{H2}^{av} [vol% dry dil.-free]		Y_{C3H8}^{av} [vol% dry dil.-free]		Y_{CO}^{av} [vol% dry dil.-free]		Y_{CO2}^{av} [vol% dry dil.-free]		Y_{CH4}^{av} [vol% dry dil.-free]	
	Mean	St.dev.	Mean	St.dev.	Mean	St.dev.	Mean	St.dev.	Mean	St.dev.	Mean	St.dev.	Mean	St.dev.	Mean	St.dev.
WSP	0.0380	0.003	0.844	0.047	81.70	9.707	32.82	1.831	3.23	0.783	38.88	0.036	12.29	0.556	12.78	1.386
WSP–T1add	0.0282	0.002	1.011	0.077	49.15	3.337	36.66	0.814	4.13	0.417	36.37	1.948	10.67	0.656	12.18	0.784
WSP–T2add	0.0299	0.002	1.041	0.120	50.31	6.323	37.70	3.889	3.48	0.153	36.26	0.798	10.33	1.466	12.24	2.089
WSP–T3add	0.0311	0.003	1.006	0.171	50.64	3.011	37.86	4.153	3.13	0.635	37.91	3.212	8.76	2.061	12.34	1.636
WSP–T1Wadd	0.0338	0.004	0.946	0.080	55.34	7.181	36.79	1.712	3.55	0.976	38.98	1.792	8.63	0.386	12.05	0.282
WSP–T2Wadd	0.0313	0.003	0.976	0.123	50.50	5.251	37.19	2.337	3.33	0.871	38.36	3.155	8.83	1.411	12.30	0.654
WSP–T3Wadd	0.0285	0.002	1.116	0.062	43.74	2.294	39.38	2.003	3.11	0.576	35.30	0.472	8.75	0.532	13.46	0.861

Table A3
Results from devolatilization tests with SIB ("Mean" = arithmetic mean out of the three experimental replications; "St.dev." = standard deviation out of the three experimental replications).

SIB 700 °C	η^{av} [mol/g biomass]		λ^{av} [mol/mol]		χ_C^{av} [%]		Y_{H2}^{av} [vol% dry dil.-free]		Y_{C3H8}^{av} [vol% dry dil.-free]		Y_{CO}^{av} [vol% dry dil.-free]		Y_{CO2}^{av} [vol% dry dil.-free]		Y_{CH4}^{av} [vol% dry dil.-free]	
	Mean	St.dev.	Mean	St.dev.	Mean	St.dev.	Mean	St.dev.	Mean	St.dev.	Mean	St.dev.	Mean	St.dev.	Mean	St.dev.
WSP	0.0174	0.001	0.262	0.070	55.46	2.955	10.12	2.232	9.89	0.246	39.00	1.831	25.65	0.685	15.33	0.286
WSP–T1add	0.0170	0.001	0.457	0.027	43.04	1.383	16.38	0.800	10.18	1.618	35.84	0.437	19.86	0.146	17.73	1.769
WSP–T2add	0.0157	0.002	0.631	0.125	37.69	5.207	20.67	3.292	9.67	1.308	32.97	1.476	18.26	0.790	18.44	2.338
WSP–T3add	0.0163	0.001	0.706	0.097	37.02	2.650	21.95	1.573	8.54	1.410	31.30	2.292	18.54	1.331	19.67	2.961
WSP–T1Wadd	0.0195	0.001	0.475	0.007	44.60	1.506	18.84	0.226	8.72	0.845	39.68	0.942	16.98	1.228	15.78	0.746
WSP–T2Wadd	0.0171	0.002	0.569	0.067	39.33	2.543	19.62	1.610	9.61	2.311	34.59	1.221	18.53	0.731	17.65	1.259
WSP–T3Wadd	0.0193	0.001	0.624	0.041	41.51	2.137	21.49	1.003	7.55	1.229	34.49	0.696	17.17	0.768	19.29	2.280
SIB 800 °C	η^{av} [mol/g biomass]		λ^{av} [mol/mol]		χ_C^{av} [%]		Y_{H2}^{av} [vol% dry dil.-free]		Y_{C3H8}^{av} [vol% dry dil.-free]		Y_{CO}^{av} [vol% dry dil.-free]		Y_{CO2}^{av} [vol% dry dil.-free]		Y_{CH4}^{av} [vol% dry dil.-free]	
	Mean	St.dev.	Mean	St.dev.	Mean	St.dev.	Mean	St.dev.	Mean	St.dev.	Mean	St.dev.	Mean	St.dev.	Mean	St.dev.
WSP	0.0281	0.004	0.673	0.040	71.40	9.063	25.55	1.636	6.42	0.957	37.98	1.235	17.31	0.504	12.74	0.982
WSP–T1add	0.0233	0.001	0.854	0.050	49.67	3.359	29.06	1.022	8.41	0.810	34.08	1.128	15.85	0.448	12.62	0.687
WSP–T2add	0.0252	0.002	0.851	0.056	51.20	1.985	29.75	2.068	6.85	0.628	34.99	2.329	15.08	1.401	13.34	2.126
WSP–T3add	0.0243	0.004	0.916	0.082	47.24	5.100	31.02	1.272	6.39	1.574	34.01	2.429	14.70	0.914	13.87	0.095
WSP–T1Wadd	0.0241	0.002	0.836	0.089	48.83	4.013	29.32	2.808	8.22	0.753	35.11	0.424	14.37	0.361	12.97	2.219
WSP–T2Wadd	0.0270	0.002	0.767	0.060	52.19	3.275	29.11	1.250	6.19	0.689	38.01	1.366	13.86	0.885	12.84	0.643
WSP–T3Wadd	0.0231	0.002	0.895	0.233	45.32	7.610	30.54	4.753	7.73	0.406	34.87	4.281	14.12	0.609	12.74	0.900

(*continued on next page*)

Table A3 (*continued*)

SIB 900 °C	η^{av} [mol/g biomass]		λ^{av} [mol/mol]		χ_C^{av} [%]		Y_{H2}^{av} [vol% dry dil.-free]		Y_{C3H8}^{av} [vol% dry dil.-free]		Y_{CO}^{av} [vol% dry dil.-free]		Y_{CO2}^{av} [vol% dry dil.-free]		Y_{CH4}^{av} [vol% dry dil.-free]	
	Mean	St.dev.	Mean	St.dev.	Mean	St.dev.	Mean	St.dev.	Mean	St.dev.	Mean	St.dev.	Mean	St.dev.	Mean	St.dev.
WSP	0.0398	0.003	0.900	0.071	82.21	4.149	36.07	2.634	3.58	1.141	40.12	1.132	10.08	0.791	10.15	1.014
WSP–T1add	0.0362	0.005	1.039	0.134	60.07	6.729	39.10	3.166	3.83	1.775	37.80	2.683	9.12	1.334	10.16	0.806
WSP–T2add	0.0346	0.004	1.120	0.055	53.61	3.016	41.76	1.971	2.93	1.204	37.32	1.540	7.57	0.988	10.42	0.743
WSP–T3add	0.0351	0.003	1.063	0.210	53.89	9.904	42.26	5.416	3.06	0.486	40.16	3.161	6.18	0.461	8.34	2.049
WSP–T1Wadd	0.0363	0.004	0.956	0.062	58.22	5.776	37.98	0.930	3.48	0.222	39.80	1.800	7.61	0.572	11.14	0.661
WSP–T2Wadd	0.0358	0.000	1.066	0.049	53.43	1.569	41.22	1.045	2.76	0.324	38.69	1.292	7.22	0.546	10.11	0.945
WSP–T3Wadd	0.0314	0.005	1.068	0.173	49.69	8.784	40.13	2.410	4.38	0.148	37.98	3.728	7.28	0.584	10.22	1.084

Table A4
Results from devolatilization tests with LD ("Mean" = arithmetic mean out of the three experimental replications; "St.dev." = standard deviation out of the three experimental replications).

LD 700 °C	η^{av} [mol/g biomass]		λ^{av} [mol/mol]		χ_C^{av} [%]		Y_{H2}^{av} [vol% dry dil.-free]		Y_{C3H8}^{av} [vol% dry dil.-free]		Y_{CO}^{av} [vol% dry dil.-free]		Y_{CO2}^{av} [vol% dry dil.-free]		Y_{CH4}^{av} [vol% dry dil.-free]	
	Mean	St.dev.	Mean	St.dev.	Mean	St.dev.	Mean	St.dev.	Mean	St.dev.	Mean	St.dev.	Mean	St.dev.	Mean	St.dev.
WSP	0.0178	0.002	0.437	0.077	55.55	4.895	13.31	1.713	10.25	0.936	30.60	1.616	30.13	0.747	15.72	0.964
WSP–T1add	0.0141	0.004	0.620	0.033	37.01	8.277	17.73	1.006	13.50	3.776	28.61	0.200	24.94	4.215	15.22	0.497
WSP–T2add	0.0169	0.002	0.711	0.144	40.13	6.122	20.88	3.015	9.36	0.920	29.60	1.626	25.03	1.221	15.12	0.628
WSP–T3add	0.0187	0.001	0.661	0.029	43.81	1.305	19.83	0.613	8.89	0.902	30.01	0.514	25.71	0.772	15.56	1.706
WSP–T1Wadd	0.0184	0.002	0.637	0.118	42.88	5.171	20.21	2.576	10.35	1.429	31.95	2.006	23.17	0.707	14.33	1.484
WSP–T2Wadd	0.0179	0.001	0.755	0.063	40.50	1.339	22.49	1.371	9.95	1.054	29.84	1.074	23.26	0.468	14.46	0.456
WSP–T3Wadd	0.0178	0.002	0.744	0.191	39.30	3.984	22.62	2.673	9.43	1.672	31.20	4.553	21.72	1.463	15.04	1.011
LD 800 °C	η^{av} [mol/g biomass]		λ^{av} [mol/mol]		χ_C^{av} [%]		Y_{H2}^{av} [vol% dry dil.-free]		Y_{C3H8}^{av} [vol% dry dil.-free]		Y_{CO}^{av} [vol% dry dil.-free]		Y_{CO2}^{av} [vol% dry dil.-free]		Y_{CH4}^{av} [vol% dry dil.-free]	
	Mean	St.dev.	Mean	St.dev.	Mean	St.dev.	Mean	St.dev.	Mean	St.dev.	Mean	St.dev.	Mean	St.dev.	Mean	St.dev.
WSP	0.0250	0.002	0.653	0.058	67.80	3.696	21.61	1.595	7.37	0.163	33.13	1.655	24.92	2.901	12.98	1.115
WSP–T1add	0.0249	0.007	0.819	0.103	51.57	13.544	28.77	2.508	7.21	2.260	35.36	3.469	15.44	0.447	13.23	1.810
WSP–T2add	0.0190	0.002	1.087	0.231	38.74	3.902	32.06	2.748	8.18	1.547	30.02	3.905	15.18	1.633	14.55	2.503
WSP–T3add	0.0204	0.001	1.312	0.128	38.18	1.781	37.25	1.830	7.87	1.247	28.52	2.382	14.18	0.815	12.18	2.084
WSP–T1Wadd	0.0250	0.003	0.883	0.037	47.86	3.375	31.43	0.447	7.09	1.506	35.65	1.851	12.77	0.369	13.06	1.027
WSP–T2Wadd	0.0200	0.005	0.810	0.292	38.89	10.469	28.77	5.281	6.20	2.659	37.63	8.859	13.03	1.998	14.37	0.852
WSP–T3Wadd	0.0219	0.001	1.167	0.287	39.55	3.201	35.84	5.004	7.26	1.131	31.29	3.614	13.63	0.925	11.98	2.107
LD 900 °C	η^{av} [mol/g biomass]		λ^{av} [mol/mol]		χ_C^{av} [%]		Y_{H2}^{av} [vol% dry dil.-free]		Y_{C3H8}^{av} [vol% dry dil.-free]		Y_{CO}^{av} [vol% dry dil.-free]		Y_{CO2}^{av} [vol% dry dil.-free]		Y_{CH4}^{av} [vol% dry dil.-free]	
	Mean	St.dev.	Mean	St.dev.	Mean	St.dev.	Mean	St.dev.	Mean	St.dev.	Mean	St.dev.	Mean	St.dev.	Mean	St.dev.
WSP	0.0419	0.000	1.031	0.034	80.68	2.548	39.80	1.692	2.90	0.460	38.60	0.384	9.08	0.967	9.63	0.954
WSP–T1add	0.0365	0.004	1.061	0.050	58.91	4.622	40.32	1.404	3.46	0.951	38.02	1.319	8.18	0.502	10.02	0.833
WSP–T2add	0.0357	0.003	1.114	0.035	55.69	2.649	42.30	1.086	3.40	0.727	37.98	1.380	7.12	0.393	9.21	1.403
WSP–T3add	0.0361	0.003	1.170	0.092	52.35	5.050	44.56	0.941	2.65	0.343	38.19	2.178	5.80	0.425	8.81	0.663
WSP–T1Wadd	0.0419	0.005	0.975	0.038	63.27	6.540	40.38	1.314	2.70	0.523	41.44	1.896	5.89	1.836	9.60	0.639
WSP–T2Wadd	0.0320	0.005	1.117	0.067	47.26	7.799	42.08	1.538	2.75	0.401	37.74	1.775	7.05	1.100	10.37	1.277
WSP–T3Wadd	0.0349	0.002	0.990	0.039	56.01	2.966	39.26	0.702	4.57	0.467	39.69	0.844	6.59	0.212	9.89	0.403

References

[1] K. Anderson, G. Peters, The trouble with negative emissions, Science 354 (2016) (1979) 182–183, https://doi.org/10.1126/science.aah4567.

[2] S.E. Tanzer, A. Ramírez, When are negative emissions negative emissions?, Energ Environ. Sci. 12 (2019) 1210–1218, https://doi.org/10.1039/c8ee03338b.

[3] IPPC, Global Warming of 1.5 °C, IPCC Special Report on the Impacts of Global Warming of 1.5°C above Pre-Industrial Levels and Related Global Greenhouse Gas Emission Pathways, in the Context of Strengthening the Global Response to the Threat of Climate Change. (2018) 1-16. https://www.ipcc.ch/sr15/ (accessed March 10, 2022).

[4] F. Creutzig, N. Ravindranath, G. Berndes, S. Bolwig, Bioenergy and climate change mitigation: an assessment, GCB Bioenergy 7 (2015) 916–944, https://doi.org/10.1111/gcbb.12205.

[5] A.V. Bridgwater, Renewable fuels and chemicals by thermal processing of biomass, Chem. Eng. J. 91 (2003) 87–102, https://doi.org/10.1016/S1385-8947(02)00142-0.

[6] A. di Giuliano, I. Funcia, R. Pérez-Vega, J. Gil, K. Gallucci, Novel application of pretreatment and diagnostic method using dynamic pressure fluctuations to resolve and detect issues related to biogenic residue ash in chemical looping gasification, Processes. 8 (2020) 1137, https://doi.org/10.3390/PR8091137.

[7] T. Mendiara, P. Gayán, F. García-Labiano, L.F. De Diego, A. Pérez-Astray, M.T. Izquierdo, A. Abad, J. Adánez, Chemical Looping Combustion of Biomass: An Approach to BECCS, Energy Procedia 114 (2017) 6021–6029, https://doi.org/10.1016/j.egypro.2017.03.1737.

[8] Y. Lin, H. Wang, Y. Wang, R. Huo, Z. Huang, M. Liu, G. Wei, Z. Zhao, H. Li, Y. Fang, Review of biomass chemical looping gasification in China, Energy Fuel 34 (2020) 7847–7862, https://doi.org/10.1021/acs.energyfuels.0c01022.

[9] T. Mendiara, F. García-Labiano, A. Abad, P. Gayán, L.F. de Diego, M.T. Izquierdo, J. Adánez, Negative CO_2 emissions through the use of biofuels in chemical looping technology: a review, Appl. Energy 232 (2018) 657–684, https://doi.org/10.1016/j.apenergy.2018.09.201.
[10] M. Qasim, M. Ayoub, N.A. Ghazali, A. Aqsha, M. Ameen, Recent advances and development of various oxygen carriers for the chemical looping combustion process: a review, Ind. Eng. Chem. Res. 60 (2021) 8621–8641, https://doi.org/10.1021/acs.iecr.1c01111.
[11] Y. de Vos, M. Jacobs, P. van der Voort, I. van Driessche, F. Snijkers, A. Verberckmoes, Development of stable oxygen carrier materials for chemical looping processes—A review, Catalysts 10 (2020) 926, https://doi.org/10.3390/catal10080926.
[12] H. Ge, W. Guo, L. Shen, T. Song, J. Xiao, Experimental investigation on biomass gasification using chemical looping in a batch reactor and a continuous dual reactor, Chem. Eng. J. 286 (2016) 689–700, https://doi.org/10.1016/j.cej.2015.11.008.
[13] O. Condori, F. García-Labiano, L.F. de Diego, M.T. Izquierdo, A. Abad, J. Adánez, Biomass chemical looping gasification for syngas production using LD Slag as oxygen carrier in a 1.5 kW_{th} unit, Fuel Process. Technol. 222 (2021), https://doi.org/10.1016/j.fuproc.2021.106963.
[14] J. Ströhle, M. Orth, B. Epple, Chemical looping combustion of hard coal in a 1 MW_{th} pilot plant using ilmenite as oxygen carrier, Appl. Energy 157 (2015) 288–294, https://doi.org/10.1016/j.apenergy.2015.06.035.
[15] F. Marx, P. Dieringer, J. Ströhle, B. Epple, Design of a 1 MW_{th} pilot plant for chemical looping gasification of biogenic residues, Energies (Basel). 14 (2021) 2581, https://doi.org/10.3390/en14092581.
[16] P. Ohlemüller, J. Ströhle, B. Epple, Chemical looping combustion of hard coal and torrefied biomass in a 1 MW_{th} pilot plant, Int. J. Greenhouse Gas Control 65 (2017) 149–159, https://doi.org/10.1016/j.ijggc.2017.08.013.
[17] F. Hildor, T. Mattisson, H. Leion, C. Linderholm, M. Rydén, Steel converter slag as an oxygen carrier in a 12 MW_{th} CFB boiler - ash interaction and material evolution, Int. J. Greenhouse Gas Control 88 (2019) 321–331, https://doi.org/10.1016/J.IJGGC.2019.06.019.
[18] A.K. Dubey, A. Samanta, P. Sarkar, M.K. Karmakar, A. Mukherjee, C. Loha, M. Kumar, S.G. Sahu, V.K. Saxena, P.K. Chatterjee, Hydrodynamic characteristics in a pilot-scale cold flow model for chemical looping combustion, Adv. Powder Technol. 29 (2018) 1499–1506, https://doi.org/10.1016/J.APT.2018.03.017.
[19] M.K. Karmakar, A.B. Datta, Hydrodynamics of a dual fluidized bed gasifier, Adv. Powder Technol. 21 (2010) 521–528, https://doi.org/10.1016/J.APT.2010.02.001.
[20] S. Li, Y. Shen, Multi-fluid modelling of hydrodynamics in a dual circulating fluidized bed, Adv. Powder Technol. 31 (2020) 2778–2791, https://doi.org/10.1016/J.APT.2020.05.010.
[21] D. Kim, Y. Won, J.H. Choi, J.B. Joo, H.J. Ryu, Effect of pressure on transport velocity in gas fluidized-beds, Adv. Powder Technol. 30 (2019) 2076–2082, https://doi.org/10.1016/J.APT.2019.06.021.
[22] D. Jansen, M. Gazzani, G. Manzolini, E. van Dijk, M. Carbo, Pre-combustion CO_2 capture, Int. J. Greenhouse Gas Control 40 (2015) 167–187, https://doi.org/10.1016/j.ijggc.2015.05.028.
[23] D.Y.C. Leung, G. Caramanna, M.M. Maroto-Valer, An overview of current status of carbon dioxide capture and storage technologies, Renew. Sustain. Energy Rev. 39 (2014) 426–443, https://doi.org/10.1016/j.rser.2014.07.093.
[24] E. Blomen, C. Hendriks, F. Neele, Capture technologies: Improvements and promising developments, Energy Procedia 1 (2009) 1505–1512, https://doi.org/10.1016/j.egypro.2009.01.197.
[25] N.M. Nguyen, F. Alobaid, P. Dieringer, B. Epple, Biomass-based chemical looping gasification: Overview and recent developments, Applied Sciences (Switzerland). 11 (2021) 7069, https://doi.org/10.3390/app11157069.
[26] J. Dai, K.J. Whitty, Chemical looping gasification and sorption enhanced gasification of biomass: a perspective, Chem. Eng. Process. - Process Intesif. 174 (2022), https://doi.org/10.1016/J.CEP.2022.108902.
[27] M. Martinelli, M.K. Gnanamani, S. LeViness, G. Jacobs, W.D. Shafer, An overview of Fischer-Tropsch Synthesis: XtL processes, catalysts and reactors, Appl. Catal. A 608 (2020), https://doi.org/10.1016/j.apcata.2020.117740.
[28] G. Weber, A. di Giuliano, R. Rauch, H. Hofbauer, Developing a simulation model for a mixed alcohol synthesis reactor and validation of experimental data in $IPSE_{pro}$, Fuel Process. Technol. 141 (2016) 167–176, https://doi.org/10.1016/j.fuproc.2015.05.024.
[29] I. Dimitriou, H. Goldingay, A.V. Bridgwater, Techno-economic and uncertainty analysis of Biomass to Liquid (BTL) systems for transport fuel production, Renew. Sustain. Energy Rev. 88 (2018) 160–175, https://doi.org/10.1016/j.rser.2018.02.023.
[30] N. Pour, Status of bioenergy with carbon capture and storage-potential and challenges, 1st edition, Elsevier, London, 2019. Doi: 10.1016/B978-0-12-816229-3.00005-3.
[31] A. Molino, V. Larocca, S. Chianese, D. Musmarra, Biofuels production by biomass gasification: a review, Energies (Basel). 11 (2018) 811, https://doi.org/10.3390/en11040811.
[32] M. Won Seo, S. Hoon Lee, H. Nam, D. Lee, D. Tokmurzin, S. Wang, Y. Kwon Park, Recent advances of thermochemical conversieon processes for biorefinery, Bioresour. Technol. 343 (2021), https://doi.org/10.1016/j.biortech.2021.126109.
[33] Concawe, Sustainable biomass availability in the EU, to 2050 - Concawe, (2021). https://www.concawe.eu/publication/sustainable-biomass-availability-in-the-eu-to-2050/ (accessed January 31, 2023).
[34] L.G. Gibilaro, Fluidization Dynamics, 1st edition, Butterworth-Heinemann, Oxford, 2010. Doi: 10.1201/9781420047509-c14.
[35] F. Scala, Particle agglomeration during fluidized bed combustion: Mechanisms, early detection and possible countermeasures, Fuel Process. Technol. 171 (2018) 31–38, https://doi.org/10.1016/j.fuproc.2017.11.001.
[36] Z. Miao, E. Jiang, Z. Hu, Review of agglomeration in biomass chemical looping technology, Fuel 309 (2022), https://doi.org/10.1016/J.FUEL.2021.122199.
[37] M. Coulson, J. Dahl, E. Gansekoele, A.V. Bridgwater, I. Obernberger L., van de Beld, Ash characteristics of perennial energy crops and their influence on thermal processing, in: in: 2nd World Conference on Biomass for Energy, Industry and Climate Protection, 2004, pp. 359–362.
[38] A. Demirbas, Combustion characteristics of different biomass fuels, Prog. Energy Combust. Sci. 30 (2004) 219–230, https://doi.org/10.1016/j.pecs.2003.10.004.
[39] B.M. Jenkins, L.L. Baxter, T.R. Miles, T.R. Miles, Combustion properties of biomass, Fuel Process. Technol. 54 (1998) 17–46, https://doi.org/10.1016/S0378-3820(97)00059-3.
[40] R. Chirone, F. Miccio, F. Scala, Mechanism and prediction of bed agglomeration during fluidized bed combustion of a biomass fuel: Effect of the reactor scale, Chem. Eng. J. 123 (2006) 71–80, https://doi.org/10.1016/j.cej.2006.07.004.
[41] A. di Giuliano, S. Lucantonio, B. Malsegna, K. Gallucci, Pretreated residual biomasses in fluidized beds for chemical looping Gasification: Experimental devolatilizations and characterization of ashes behavior, Bioresour. Technol. 345 (2022), https://doi.org/10.1016/j.biortech.2021.126514.
[42] B. Malsegna, A. di Giuliano, K. Gallucci, Experimental study of absorbent hygiene product devolatilization in a bubbling fluidized bed, Energies (Basel). 14 (2021) 2399, https://doi.org/10.3390/en14092399.
[43] S. Lucantonio, A. di Giuliano, K. Gallucci, Influences of the pretreatments of residual biomass on gasification processes: Experimental devolatilizations study in a fluidized bed, Appl. Sci. (Switzerland). 11 (2021) 5722, https://doi.org/10.3390/app11125722.
[44] A. di Giuliano, M. Gallucci, B. Malsegna, S. Lucantonio, K. Gallucci, Pretreated residual biomasses in fluidized beds for chemical looping gasification: Analysis of devolatilization data by statistical tools, Bioresour Technol Rep. 17 (2022), https://doi.org/10.1016/j.biteb.2021.100926.
[45] M. Barbanera, I.F. Muguerza, Effect of the temperature on the spent coffee grounds torrefaction process in a continuous pilot-scale reactor, Fuel 262 (2020), https://doi.org/10.1016/J.FUEL.2019.116493.
[46] Y. Fan, N. Tippayawong, G. Wei, Z. Huang, K. Zhao, L. Jiang, A. Zheng, Z. Zhao, H. Li, Minimizing tar formation whilst enhancing syngas production by integrating biomass torrefaction pretreatment with chemical looping gasification, Appl. Energy 260 (2020), https://doi.org/10.1016/J.APENERGY.2019.114315.
[47] R. Zhang, J. Zhang, W. Guo, Z. Wu, Z. Wang, B. Yang, Effect of torrefaction pretreatment on biomass chemical looping gasification (BCLG) characteristics: Gaseous products distribution and kinetic analysis, Energy Convers Manag. 237 (2021), https://doi.org/10.1016/J.ENCONMAN.2021.114100.
[48] T.R. Sarker, S. Nanda, A.K. Dalai, V. Meda, A Review of Torrefaction Technology for Upgrading Lignocellulosic Biomass to Solid Biofuels, BioEnergy Research 2020 14:2. 14 (2021) 645-669. Doi: 10.1007/S12155-020-10236-2.
[49] K. Cen, J. Zhang, Z. Ma, D. Chen, J. Zhou, H. Ma, Investigation of the relevance between biomass pyrolysis polygeneration and washing pretreatment under different severities: Water, dilute acid solution and aqueous phase bio-oil, Bioresour. Technol. 278 (2019) 26–33, https://doi.org/10.1016/J.BIORTECH.2019.01.048.
[50] A. Singhal, J. Konttinen, T. Joronen, Effect of different washing parameters on the fuel properties and elemental composition of wheat straw in water-washing pre-treatment. Part 2: Effect of washing temperature and solid-to-liquid ratio, Fuel 292 (2021), https://doi.org/10.1016/J.FUEL.2021.120209.
[51] A. Singhal, J. Konttinen, T. Joronen, Effect of different washing parameters on the fuel properties and elemental composition of wheat straw in water-washing pre-treatment. Part 1: Effect of washing duration and biomass size, Fuel 292 (2021), https://doi.org/10.1016/J.FUEL.2021.120206.
[52] M. Holubcik, J. Jandacka, Mathematical model for prediction of biomass ash melting temperature using additives, Komunikacie. 16 (2014) 48–53, https://doi.org/10.26552/COM.C.2014.3A.48-53.
[53] CLARA - Chemical looping gasification for sustainable production of biofuels, (n.d.). https://clara-h2020.eu/ (accessed July 7, 2020).
[54] A. di Giuliano, S. Capone, M. Anatone, K. Gallucci, Chemical looping combustion and gasification: a review and a focus on European research projects, Ind. Eng. Chem. Res. 61 (2022) 14403–14432, https://doi.org/10.1021/ACS.IECR.2C02677/ASSET/IMAGES/LARGE/IE2C02677_0004.JPEG.
[55] H. Ge, W. Guo, L. Shen, T. Song, J. Xiao, Biomass gasification using chemical looping in a 25 kW_{th} reactor with natural hematite as oxygen carrier, Chem. Eng. J. 286 (2016) 174–183, https://doi.org/10.1016/J.CEJ.2015.10.092.
[56] G. Huijun, S. Laihong, F. Fei, J. Shouxi, Experiments on biomass gasification using chemical looping with nickel-based oxygen carrier in a 25 kW_{th} reactor, Appl. Therm. Eng. 85 (2015) 52–60, https://doi.org/10.1016/J.APPLTHERMALENG.2015.03.082.
[57] V. Belgiorno, G. De Feo, C. Della Rocca, R.M.A. Napoli, Energy from gasification of solid wastes, Waste Manag. 23 (2003) 1–15, https://doi.org/10.1016/S0956-053X(02)00149-6.
[58] N. Jand, P.U. Foscolo, Decomposition of wood particles in fluidized beds, Ind. Eng. Chem. Res. 44 (2005) 5079–5089, https://doi.org/10.1021/ie040170a.

[59] T. Milne, F. Agblevor, M. Davis, S. Deutch, D. Johnson, A Review of the Chemical Composition of Fast-Pyrolysis Oils from Biomass, in: Developments in Thermochemical Biomass Conversion, Springer Netherlands, 1997: pp. 409-424. Doi: 10.1007/978-94-009-1559-6_32.
[60] K.M. Bryden, M.J. Hagge, Modeling the combined impact of moisture and char shrinkage on the pyrolysis of a biomass particle, Fuel 82 (2003) 1633–1644, https://doi.org/10.1016/S0016-2361(03)00108-X.
[61] A. di Giuliano, S. Lucantonio, K. Gallucci, Devolatilization of residual biomasses for chemical looping Gasification in Fluidized Beds Made up of Oxygen-Carriers, Energies (Basel). 14 (2021) 311, https://doi.org/10.3390/en14020311.
[62] M.G. Grønli, G. Várhegyi, C. Di Blasi, Thermogravimetric analysis and devolatilization kinetics of wood, Ind. Eng. Chem. Res. 41 (2002) 4201–4208, https://doi.org/10.1021/ie0201157.
[63] J. Rath, G. Steiner, M.G. Wolfinger, G. Staudinger, Tar cracking from fast pyrolysis of large beech wood particles, J. Anal. Appl. Pyrol. 62 (2002) 83–92, https://doi.org/10.1016/S0165-2370(00)00215-1.
[64] J.A. Conesa, A. Marcilla, J.A. Caballero, R. Font, Comments on the validity and utility of the different methods for kinetic analysis of thermogravimetric data, J. Anal. Appl. Pyrol. 58–59 (2001) 617–633, https://doi.org/10.1016/S0165-2370(00)00130-3.
[65] K. Gallucci, N. Jand, P.U. Foscolo, M. Santini, Cold model characterisation of a fluidised bed catalytic reactor by means of instantaneous pressure measurements, Chem. Eng. J. 87 (2002) 61–71, https://doi.org/10.1016/S1385-8947(01)00202-9.
[66] K. Gallucci, L.G. Gibilaro, Dimensional Cold-Modeling Criteria for Fluidization Quality, ACS Publications. 44 (2005) 5152–5158, https://doi.org/10.1021/ie049407t.
[67] M.F. Llop, N. Jand, K. Gallucci, F.X. Llauró, Characterizing gas-solid fluidization by nonlinear tools: Chaotic invariants and dynamic moments, Chem. Eng. Sci. 71 (2012) 252–263, https://doi.org/10.1016/j.ces.2011.12.031.
[68] F. Johnsson, R.C. Zijerveld, J.C. Schouten, C.M. Van Den Bleek, B. Leckner, Characterization of fluidization regimes by time-series analysis of pressure fluctuations, Int. J. Multiph. Flow 26 (2000) 663–715, https://doi.org/10.1016/S0301-9322(99)00028-2.
[69] H. Kage, M. Agari, H. Ogura, Y. Matsuno, Frequency analysis of pressure fluctuation in fluidized bed plenum and its confidence limit for detection of various modes of fluidization, Adv. Powder Technol. 11 (2000) 459–475, https://doi.org/10.1163/156855200750172060.
[70] J. Gómez-Hernández, D. Serrano, A. Soria-Verdugo, S. Sánchez-Delgado, Agglomeration detection by pressure fluctuation analysis during Cynara cardunculus L. gasification in a fluidized bed, Chem. Eng. J. 284 (2016) 640–649, https://doi.org/10.1016/j.cej.2015.09.044.
[71] M. Fiorentino, A. Marzocchella, P. Salatino, Segregation of fuel particles and volatile matter during devolatilization in a fluidized bed reactor - II, Experimental, Chem Eng Sci. 52 (1997) 1909–1922, https://doi.org/10.1016/S0009-2509(97)00019-5.
[72] J.C. Schouten, C.M. van den Bleek, Monitoring the quality of fluidization using the short-term predictability of pressure fluctuations, AIChE J 44 (1998) 48–60, https://doi.org/10.1002/aic.690440107.
[73] J. Nijenhuis, R. Korbee, J. Lensselink, J.H.A. Kiel, J.R. van Ommen, A method for agglomeration detection and control in full-scale biomass fired fluidized beds, Chem. Eng. Sci. 62 (2007) 644–654, https://doi.org/10.1016/j.ces.2006.09.041.
[74] S.M. Okhovat-Alavian, J. Behin, N. Mostoufi, Investigating the flow structures in semi-cylindrical bubbling fluidized bed using pressure fluctuation signals, Adv. Powder Technol. 30 (2019) 1247–1256, https://doi.org/10.1016/J.APT.2019.04.004.
[75] F. Lebendig, I. Funcia, R. Pérez-Vega, M. Müller, Investigations on the Effect of Pre-Treatment of Wheat Straw on Ash-Related Issues in Chemical Looping Gasification (CLG) in Comparison with Woody Biomass, Energies 2022, Vol. 15, Page 3422. 15 (2022) 3422. Doi: 10.3390/EN15093422.
[76] L. Shadle, F luidized B ed C hemical L ooping (2006) 4056–4060.
[77] P. Dieringer, I. Funcia, A. Soleimani, T. Liese, Public Report II (2020).
[78] N.M. Nguyen, F. Alobaid, B. Epple, Chemical looping gasification of torrefied woodchips in a bubbling fluidized bed test rig using iron-based oxygen carriers, Renew, Energy 172 (2021) 34–45, https://doi.org/10.1016/j.renene.2021.03.006.
[79] O. Condori, F. García-Labiano, L.F. de Diego, M.T. Izquierdo, A. Abad, J. Adánez, Biomass chemical looping gasification for syngas production using ilmenite as oxygen carrier in a 1.5 kW_{th} unit, Chem. Eng. J. 405 (2021), https://doi.org/10.1016/j.cej.2020.126679.
[80] T. Mattison, F. Hildor, Y. Li, C. Linderholm, Negative emissions of carbon dioxide through chemical-looping combustion (CLC) and gasification (CLG) using oxygen carriers based on manganese and iron, Mitig Adapt Strateg Glob Chang. 25 (2020) 497–517, https://doi.org/10.1007/s11027-019-09860-x.
[81] F. Hildor, H. Leion, C.J. Linderholm, T. Mattisson, Steel converter slag as an oxygen carrier for chemical-looping gasification, Fuel Process. Technol. 210 (2020), https://doi.org/10.1016/j.fuproc.2020.106576.
[82] M. Luise, M. Vitetta, G. Bacci, F. Zuccardi Merli, Teoria dei segnali, 3rd edition,, The McGraw-Hill Companies, New York, 2009.
[83] D. Wilkinson, Determination of minimum fluidization velocity by pressure fluctuation measurement, Can. J. Chem. Eng. 73 (1995) 562–565, https://doi.org/10.1002/cjce.5450730416.
[84] J. Xiang, Q. Li, A. Wang, Y. Zhang, Mathematical analysis of characteristic pressure fluctuations in a bubbling fluidized bed, Powder Technol. 333 (2018) 167–179, https://doi.org/10.1016/j.powtec.2018.04.030.
[85] L.T. Fan, T.-C. Ho, S. Hiraoka, W.P. Walawender, Pressure fluctuations in a fluidized bed, AIChE J 27 (1981) 388–396, https://doi.org/10.1002/aic.690270308.
[86] J. Van Der Schaaf, J.C. Schouten, C.M. Van Den Bleek, Origin, propagation and attenuation of pressure waves in gas-solid fluidized beds, Powder Technol. 95 (1998) 220–233, https://doi.org/10.1016/S0032-5910(97)03341-X.
[87] J. Fuchs, J.C. Schmid, S. Müller, A.M. Mauerhofer, F. Benedikt, H. Hofbauer, The impact of gasification temperature on the process characteristics of sorption enhanced reforming of biomass, Biomass Convers. Biorefin. 10 (2020) 925–936, https://doi.org/10.1007/S13399-019-00439-9/FIGURES/10.
[88] B. Ru, S. Wang, G. Dai, L. Zhang, Effect of Torrefaction on Biomass Physicochemical Characteristics and the Resulting Pyrolysis Behavior, Energy Fuel 29 (2015) 5865–5874, https://doi.org/10.1021/ACS.ENERGYFUELS.5B01263/ASSET/IMAGES/MEDIUM/EF-2015-012639_0006.GIF.
[89] Z. Zhang, S. Pang, Experimental investigation of biomass devolatilization in steam gasification in a dual fluidised bed gasifier, Fuel 188 (2017) 628–635, https://doi.org/10.1016/J.FUEL.2016.10.074.
[90] D. Medic, M. Darr, A. Shah, B. Potter, J. Zimmerman, Effects of torrefaction process parameters on biomass feedstock upgrading, Fuel 91 (2012) 147–154, https://doi.org/10.1016/J.FUEL.2011.07.019.
[91] Q. Chen, J.S. Zhou, B.J. Liu, Q.F. Mei, Z.Y. Luo, Influence of torrefaction pretreatment on biomass gasification technology, Chinese Science Bulletin 2011 56:14. 56 (2011) 1449-1456. Doi: 10.1007/S11434-010-4292-Z.
[92] Pine Wood Pellet, (2020). https://pinewoodpellet.com/ (accessed July 12, 2022).
[93] N. Nemati, R. Zarghami, N. Mostoufi, Investigation of Hydrodynamics of High-Temperature Fluidized Beds by Pressure Fluctuations, Chem. Eng. Technol. 39 (2016) 1527–1536, https://doi.org/10.1002/CEAT.201500443.